since 1961

Baltica

BALTICA Volume 32 Number 1 June 2019: 107–126

https://doi.org/10.5200/baltica.2019.1.9

Petrography and mineral chemistry of the Varena Iron Ore deposit, southeastern Lithuania: implications for the evolution of carbonate and silicate rocks and ore mineralization

Gražina Skridlaitė, Laurynas Šiliauskas, Sabina Prušinskienė and Bogusław Bagiński

Skridlaitė, G., Šiliauskas L., Prušinskienė S., Bagiński B. 2019. Petrography and mineral chemistry of the Varena Iron Ore deposit, southeastern Lithuania: implications for the evolution of carbonate and silicate rocks and ore mineralization. *Baltica, 32 (1)*, 107–126. Vilnius. ISSN 0067-3064.
Manuscript submitted 10 February 2019 / Accepted 23 May 2019 / Published online 20 June 2019

Abstract. The large Varena Iron Ore deposit of southeast Lithuania lies beneath 200–400 m thick sedimentary cover in the East European Craton. Several drilling projects have revealed that it contains ca. 70–200 million tons of iron ore. A metasomatic origin has been proposed by several investigators, with an igneous (mafic, ultramafic carbonatitic) origin also considered. Detailed micropetrography on a variety of ore-bearing and skarnitised samples through backscattered electron imaging, along with mineral chemical analysis and monazite dating by electron microprobe, provide support for a metasomatic origin. High-grade temperature (ca. 700–750° C) skarns containing forsterite, enstatite, spinel and diopside were formed preferentially in carbonate-rich rocks and were subsequently overprinted by amphibole-bearing (tremolite, actinolite, anthophyllite and hornblende) skarns. A low-temperature hydrous influx and changing redox conditions not only caused the serpentinization of the earlier skarns, but also deposited a considerable amount of iron ore in the form of magnetite. Iron was derived from various sources and was accompanied by sulphide, apatite, REE and other mineralizations. The ca. 1.78 Ga monazite grew during the regional metamorphism, while ca. 1.54 Ga is attributed to the last mineralization phases.

Keywords: *Varena Iron Ore deposit; metasomatism; skarn; iron ore; monazite dating*

✉ *Gražina Skridlaitė (grazina.skridlaite@gamtc.lt), Nature Research Centre, Akademijos 2, LT-08412 Vilnius, Lithuania, Laurynas Šiliauskas (laurynas.siliauskas@gamtc.lt), Nature Research Centre, Akademijos 2, LT-08412 Vilnius, Lithuania, Sabina Prušinskienė (sabina.prusinskiene@gamtc.lt), Nature Research Centre, Akademijos 2, LT-08412 Vilnius, Lithuania, Bogusław Bagiński (B.baginski1@uw.edu.pl), Institute of Geochemistry, Mineralogy and Petrology, Faculty of Geology of the University of Warsaw, Al. Żwirki i Wigury, 93, PL-02-089 Warszawa, Poland*

INTRODUCTION

In the western East European Craton (EEC) that underlies Lithuania and parts of neighboring countries, a Precambrian basement is buried beneath Paleozoic, Mesozoic and Quaternary sediments. In Lithuania, the thickness of sedimentary cover drops from 2000 m in the west to ca. 200 m in the southwest. In southeastern Lithuania, drilling of magnetic anomalies in the shallowest cover, revealed the presence of rich iron ores. In 1982–1988, geological/geophysical investigations were carried out and the Varena Iron Ore Deposit (VIOD) was established. The deposit was estimated at approximately 1.8 million tons of iron ore (e.g. Marfin *et al.* 1988). In 1990–1992, an additional drilling project (eight more drillings) revealed several more iron ore bodies, raising the potential iron resources to 71 or 219.6 million tons according to differing economic evaluations (e.g. Marfinas 1996 and 1998).

A sedimentary origin for the dolomite marbles that host rocks of the ore deposit was suggested by Skridlaite (1993a, b) and Skridlaite, Motuza (2001), based on low trace element and REE contents. This was supported by interlayering with metasediments and metavolcanics, including metagreywackes and amphibolites, along with a variety of schists and gneisses. A metasomatic origin for the iron ores and the host mineral assemblages that include forsterite, diopside, tremolite and serpentine was proposed by Motuza *et al.* (1989) and Klein *et al.* (1990). A more detailed description of skarns, metasomatites and ores in the VIOD is provided by Skridlaite (1993a, b). Alternative magmatic models for the origin of the VIOD were later proposed, where the deposit forms part of a layered mafic complex (Kepežinskas, Šliaupa 1994), or of carbonatite (Kirkliauskaite *et al.* 2016) or ultramafic (Motuza, Kirkliauskaite 2016) intrusions.

Considering that the VIOD is the largest mineral deposit discovered to date in the crystalline basement of Lithuania, and that the origin of the deposit is of first-order importance for mineral exploration, new information on the composition and mechanisms of mineralization is of great value. In previous studies, only limited petrographic and mineralogical information has been provided. The present study presents results of a detailed examination of the VIOD rocks by Scanning Electron Microscopy (SEM) with Energy Dispersive (EDS) and Wavelength Dispersive (WDS) Spectrometry. This is combined with mineral chemistry and chemical dating of monazite by electron microprobe to provide evidence for the metasomatic origin and evolution of the deposit.

Geological setting

The western part of the EEC basement in Lithuania consists of Palaeoproterozoic arcuate domains: the Belarus-Podlasie Granulite (BPG), and the Latvian-East-Lithuanian (LEL), Mid-Lithuanian (MLD) and West Lithuanian Granulite (WLG). These are intruded by Mesoproterozoic plutons (Fig. 1, Bogdanova *et al.* 2015). The LEL belongs to the large Bergslagen – Livonia megadomain, extending from eastern Lithuania through Latvia and Estonia to central Sweden. The MLD is part of the larger Mid-Baltic Belt, whereas the WLG together with the Polish basement comprise the Amberland (Bogdanova *et al.* 2015). The LEL formed during the Svecofennian orogeny, with the oldest continental crust of Lithuania generated at ca. 1.89–1.87 Ga (Bogdanova *et al.* 2015). The crust and later volcano-sedimentary complexes (former fore-arcs, back arcs etc.) were intruded by 1.84–1.86 Ga gabbro-diorite-granodiorite magmatic bodies, by which time a continental margin had been established (Bogdanova *et al.* 2015). Resumed subduction at ca. 1.83 Ga produced more volcano-sedimentary complexes (Siliauskas *et al.* 2018a) to the present west of the VIOD. All the complexes were affected a different degrees by several metamorphic episodes between 1.80 and 1.50 Ga (Bogdanova *et al.* 2001, Skridlaite *et al.* 2014). The continental crust was intruded by the Mesoproterozoic (ca. 1.53–1.50 Ga) Anorthosite-Mangerite-Charnockite-Granite (AMCG) Mazury complex (see Skridlaite *et al.* 2003) and the Kabeliai granites (Sundblad *et al.* 1994).

The VIOD (Fig. 2) is hosted for the most part in metasedimentary rocks surrounded by metaigneous rocks of felsic, intermediate and mafic composition. It is assumed that carabonate rocks, predominantly dolostones, were accumulated in a shelf environment along an established continental margin, presumably after 1.86–1.84 Ga (Bogdanova *et al.* 2015). These were pure dolostones or contained variable amounts of chert and clastic sediment (sand and clay) layers. Metagraywacke layers adjacent to dolostones contain ca. 2.0 Ga detrital zircon and were metamorphosed at ca. 1.80 Ga (Mansfeld 2001). Metapelite and magnetite-quartzite (chert) bodies occur to the east of the VIOD (Skridlaite, Motuza 2001). Plastically deformed and metamorphosed rocks of granitic, dioritic and gabbroic compositions, dated at 1.87–1.90 Ga (Siliauskas *et al.* 2018b), underlay the VIOD rocks.

Methods of investigation

After careful examination of the VIOD rocks, the most representative sections of the Dzukija 7 (D7), Dzukija 8 (D8) and Varena 982 (982) drill cores, taken from the flanks of different iron ore bodies (Fig. 2) were chosen for detailed study. More than 40 polished thin sections were prepared at Warsaw University in Poland. On the basis of a detailed field, microscopic (over one hundred thin sections were examined under a Nicon 50iPOL polarizing microscope), chemical (whole rock analyses) investigations, three core sections were compiled (Fig. 3). Polished thin sections from representative intervals were studied by Scanning Electron Microscope (SEM) using the Quanta 250 instrument at the Open Access Centre (OAC) of the Nature Research Centre in Vilnius. Images were taken using a backscattered electron detector (BSE). The chemical composition of rock-forming minerals was obtained by the EDS detector X-Max, the INCA x-stream digital pulse processor and the INCA Energy EDS software. The X-Max (large area) 20 mm^2 silicon drift detector (SDD) is liquid and nitrogen-free. Chemical analysis was conducted by electron beam with an operating current of 1.1–1.2 nA and accelerating voltage of 10–20 kV. Magnetite compositions were obtained by the Cameca SX100 electron microprobe analyzer (EMPA) at the Institute of Geochemistry, Mineralogy and Petrology, Warsaw University, Poland, using 15 nA current and voltage of 20 kV. Representative mineral analyses are presented in the Supporting Online Material (Table S1).

Chemical dating of monazite from core sample 982-4 (418.2 m) was carried out at Warsaw University, Faculty of Geology, by EPMA in the Cameca SX100 facility, using natural mineral and synthetic standards. An accelerating voltage of 20 kV and beam current of 60 nA were used. The following lines were used in quantitative analysis: Kα lines of P, La, Ca, S and Si; Lα lines of Ce, Er, Yb and Y; Lβ lines of

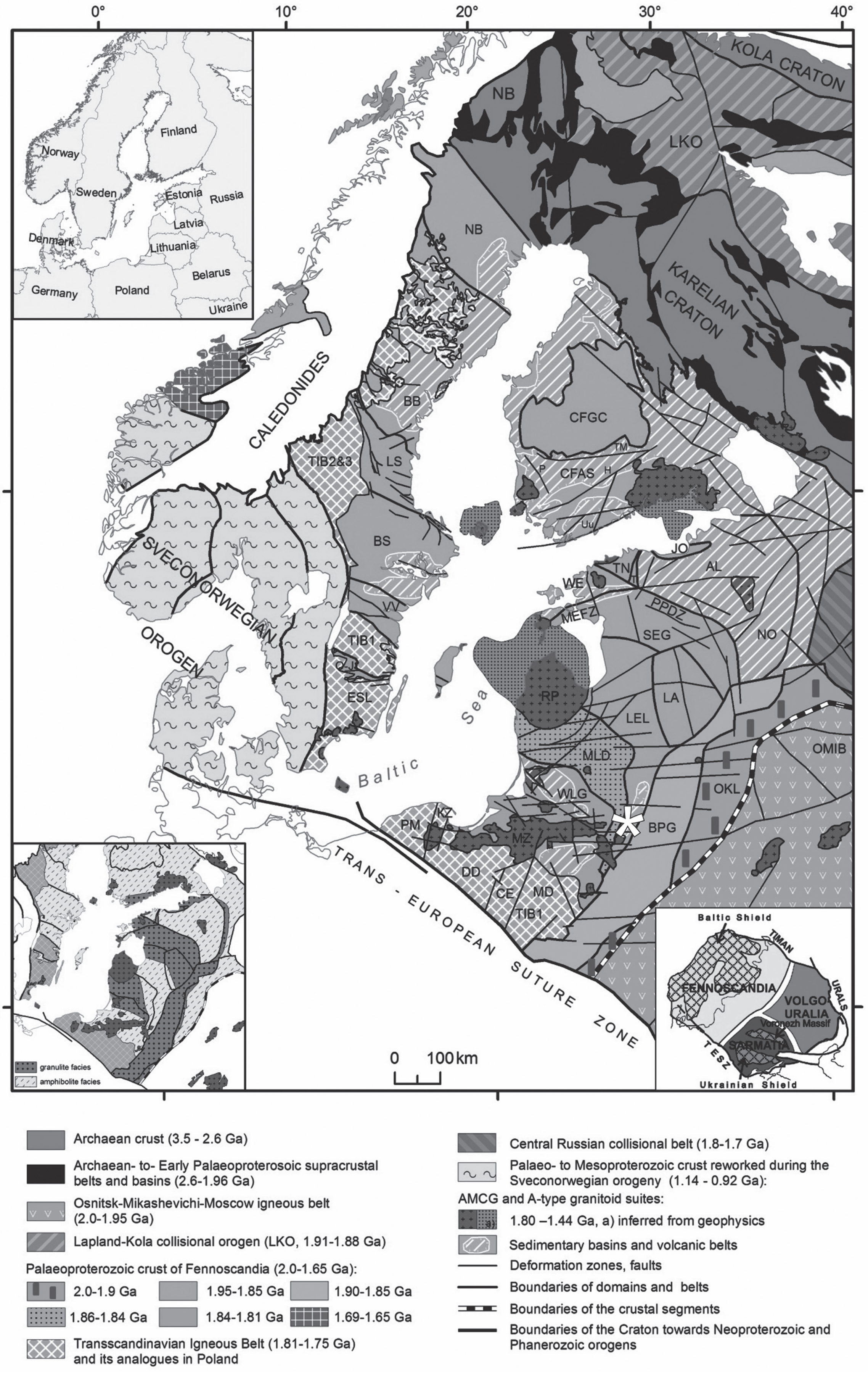

Fig. 1 Major Palaeoproterozoic tectonic domains in the Baltic Sea area (after Bogdanova *et al*. 2015). White star indicates the study area

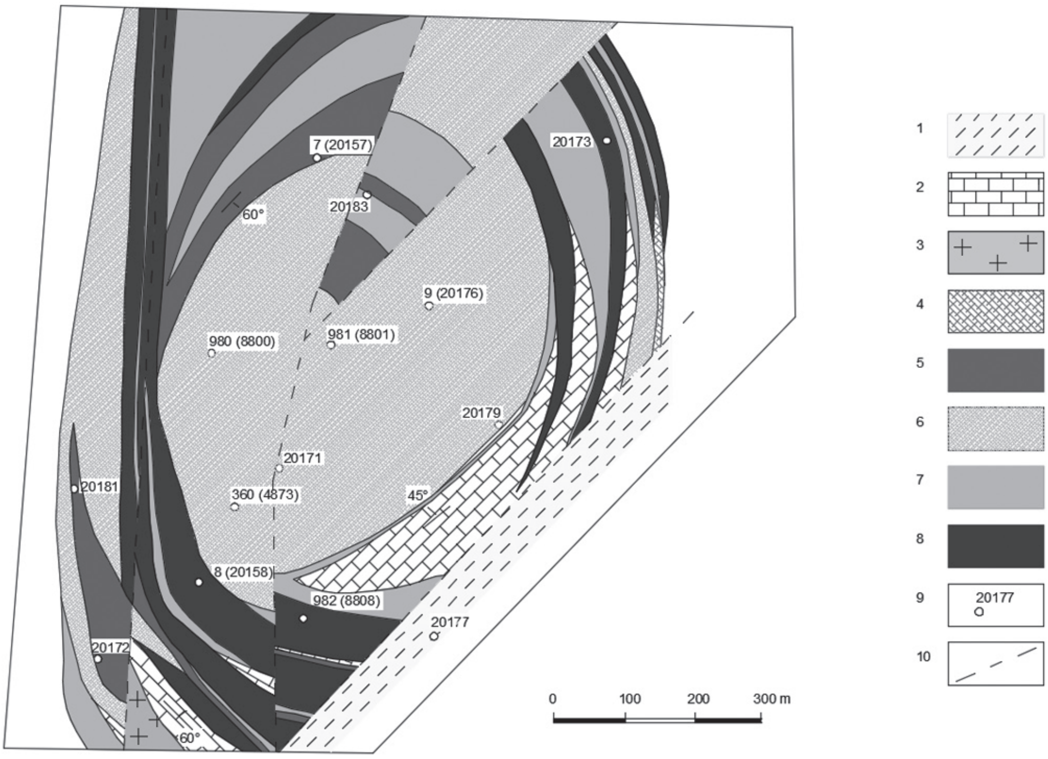

Fig. 2 Geological sketch map of the Varėna Iron Ore Deposit (VIOD): (1) plagiogneiss and gneiss; (2) marble and calciphyre; (3) Bt-, Bt–Am granitoids and granitogneisses; (4) Px-, Am–Px-, and Scp–Px rocks; (5) Am-, Px–Am-, Scp–Am rocks, Phl–Am rocks with Mag, Ap and sulfides; (6) Pl-, Scp–Pl-, Pl–Scp-, Qtz–Mc–Pl rocks; (7) Srp-, Am–Srp-, Mag–Srp rocks; (8) Mag rocks (ores); (9) location of boreholes; (10) faults

Pr, Nd, Sm, Gd, Tb, Dy and Ho; Mβ lines of Pb and U; Mα line of Th. The ages of individual point analyses were calculated using the correction presented by Montel *et al*. (1996) and analyzed using the Isoplot 3.75 (Ludwig 2012) add-in for Excel (Table S2).

Sample description

The term “skarn” is here used in a non-genetic sense, referring to carbonate–silicate rocks dominated by olivine, enstatite, clinopyroxene, amphibole, serpentine and talc.

The 982 cross-section (Fig. 3A) consists of carbonates with or without the presence of skarn minerals (394–418; 590–723, 749–755 m); magnetite-enriched serpentine and iddingsite rock with relics of olivine and spinel (418–590 m); metasomatised amphibole-bearing gneisses and amphibolites with granite veinlets and unaltered amphibolite intervals (755–900 m).

To study a contact between skarn in carbonate rock and magnetite ore, a sample of thin-layered magnetite ore (**982-3**) and of skarn (**982-4**) were taken from a 4-cm interval at a depth of 418.7 m. Sample 982-3 consists of (1) laminations of magnetite (with rare magnetite-baddeleyite intergrowths) interlayered with carbonate (mostly calcite) containing rare monazite along with 0.5–1 mm-sized serpentine grains (Fig. 4A), (2) carbonate laminations with irregular clots of serpentine, and (3) stripes of magnetite intergrown with carbonates, spinel, chlorite, olivine and other minerals. Sample 982–4 exhibits a fine-grained carbonate (calcite and dolomite) matrix with mostly rounded, 0.1–1 mm-sized clots of multiple serpentines and carbonates. A **982-6** sample was taken from the purest marble at 598.1 m. The almost pure dolomite marble with rare round olivine grains and phlogopite flakes has fractures filled with serpentine and phlogopite. A breccia-like magnetite ore was sampled at 600.2 m (**982-7**). Domains of calcite and elongated tremolite grains alternate with large magnetite grains in a matrix of various serpentines, iddingsite, phlogopite flakes, tremolite, calcite and finer-grained interstitial magnetite (Fig. 4B). Tremolite gradually becomes more abundant downwards and constitutes a monomineralic zone more than a meter-thick from 603.8 m (sample **982-9**). Elongated tremolite grains are commonly fractured, and fractures are filled with serpentines. The number of fractures increase with depth until they form a dense network (Fig. 4C). Magnetite grains appear in the serpentine-rich areas, grow in number and form massive ore at ca. 605 m. Bunches of chlorite flakes occur in serpentine-rich areas. A sample of diopside skarn (**982-616**) was taken from an interval between 613 and 617 m. The skarn consists of prismatic diopside grains with numerous cracks filled with serpentine and iddingsite

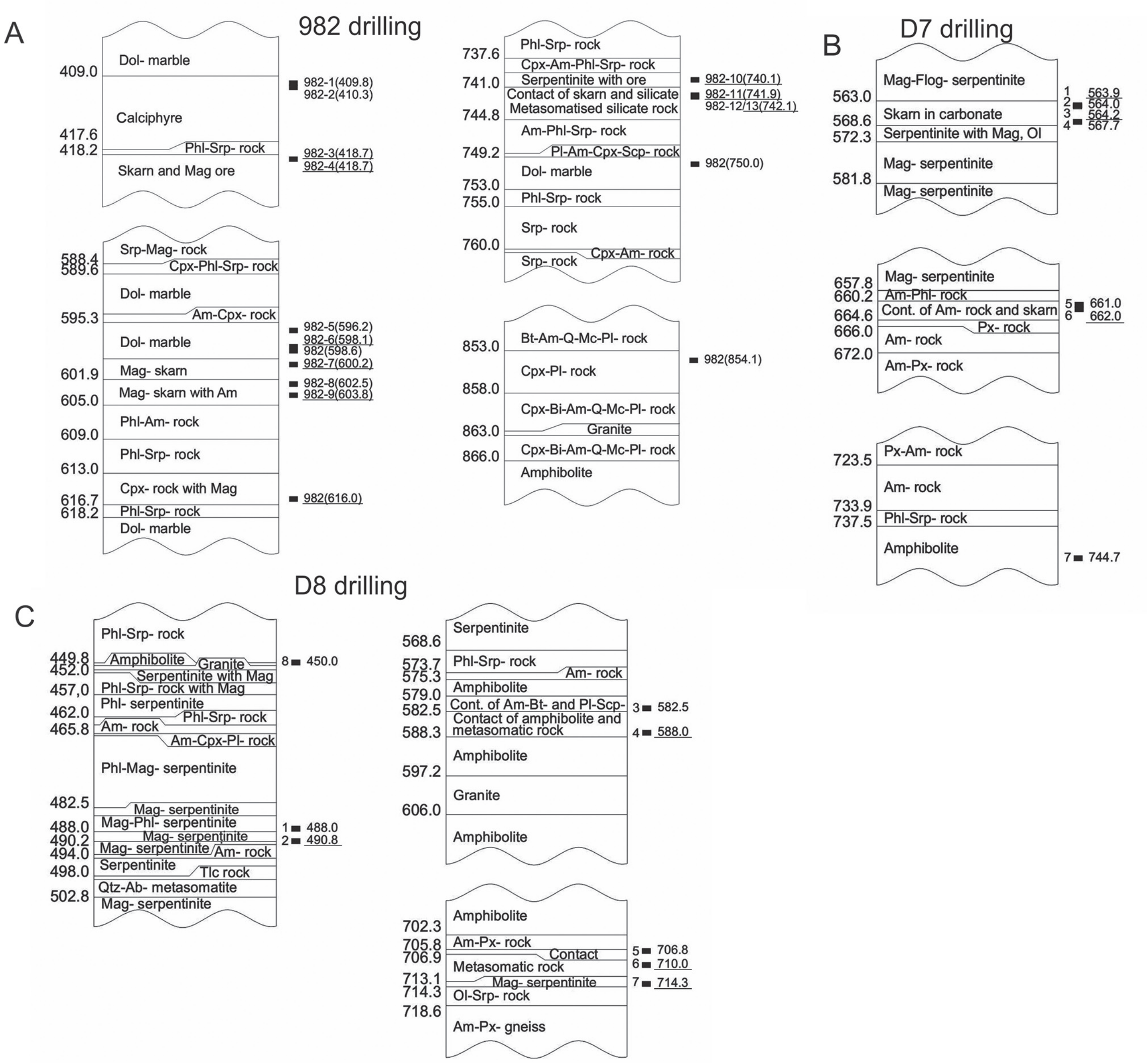

Fig. 3 Cross-sections of the host rocks and iron ores from the 982 (A), D7 (B) and D8 (C) drillings with a location of the studied samples underlined

(Fig. 4D), the latter surrounding magnetite grains and intimately intergrown with chalcopyrite and pentlandite. Magnetite fills some interstices between diopside grains (Fig. 4D). In **982-10** (740.1 m), serpentines either form round pseudomorphs after olivine or layers between spinel and magnetite grains. Magnetite fills fractures together with serpentine and chlorite or forms euhedral crystals and larger crystal aggregates (Fig. 4E). A sample (**982-11**) from 741.9 m is thinly zoned with layers of metasomatized amphibolite, and a rock made from serpentine-dominated patches surrounded by amphibole. The latter is from the contact with a magnetite ore interval (Fig. 3A). The contact is not sharp, intergrown. Phlogopite flakes and single apatite grains are associated with the hornblende rock. Amphiboles surrounding serpentine patches are mostly tremolite. Iddingsite is associated with serpentine. A tiny broken calcite veinlet cross-cuts the rock. Sample **982-13** was taken from an amphibolite with diopside patches and clots along the fractures at 742.1 m (Fig. 4F). The least altered part consists of hornblende, plagioclase, titanomagnetite, titanite and apatite. Fractures are mostly filled with calcite, natrolite and analcime.

The investigated part of the **D7 profile** (Fig. 3B) comprises magnetite ores (560–660 m) with intervals of carbonates and skarns (563–572, 660–662 m), metasomatized alumina-silicate rocks (572–737.5 m) and amphibolite (from 737.5 m).

Samples **D7-1** (563.9 m) and **D7-3** (564.2) display a wide variety of skarn minerals. In both samples, some indications of a primary zonation were obscured by later brecciation that produced a patchy texture in the rock (Fig. 4G). Olivine-rich patches alternate with tremolite-rich zones, and iddingsite aggregates mostly outline the contacts. Apatite is abundant in the tremolite zones. Serpentine fills intragranular spaces and cracks. In the olivine-rich domains, magnetite togeth-

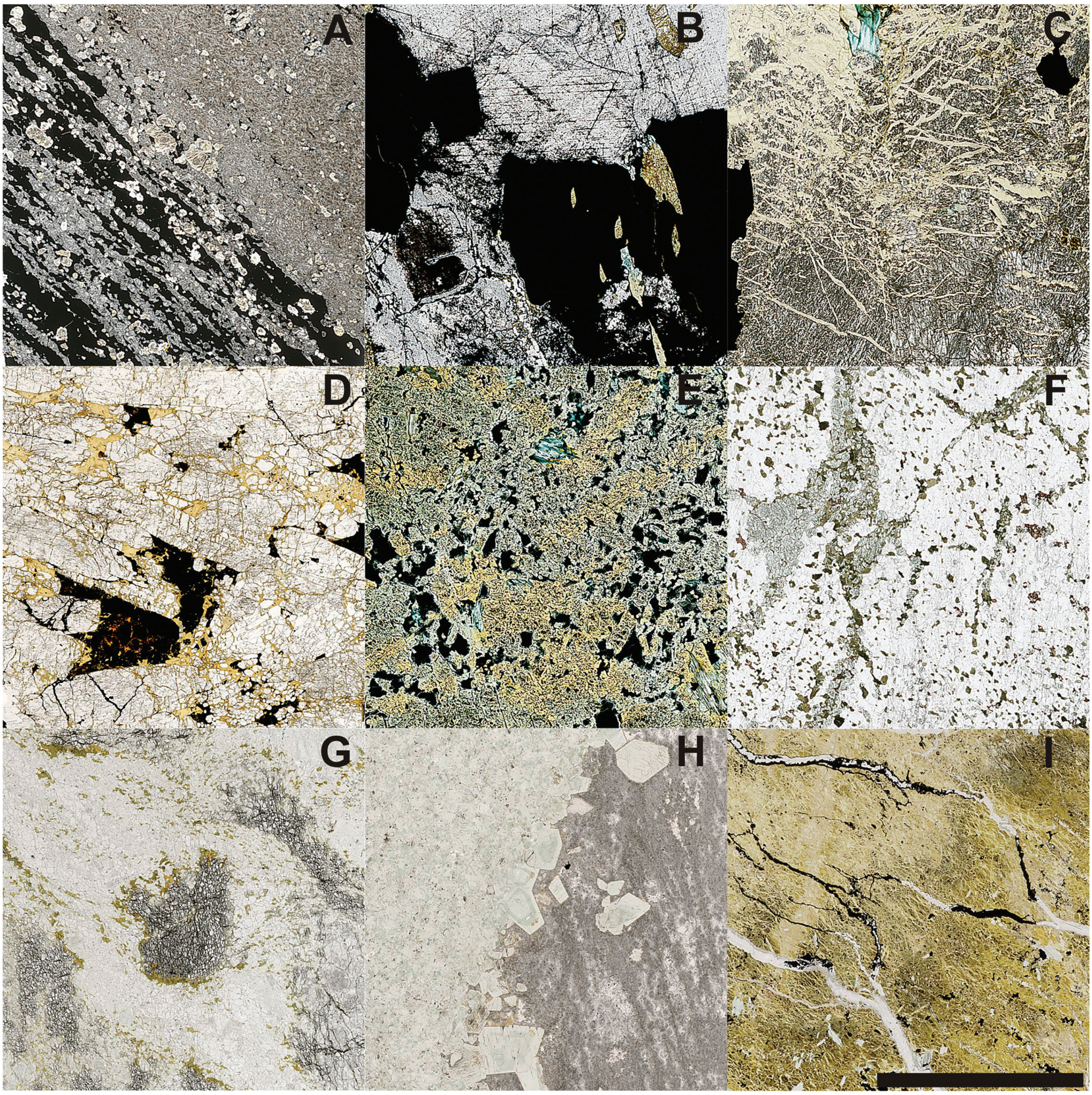

Fig. 4 Microphotographs of the studied samples: (A) thin-layered magnetite (black) and carbonates (grey) with serpentine (greenish) spots (982-3); (B) brecciated ore consisting of grey calcite (with well pronounced cleavage planes) and elongated tremolite (olive-green) grains (upper part), and magnetite grains (black) in a matrix of fine-grained calcite, serpentines, magnetite, iddingsite and phlogopite (bluish-green) flakes (lower part) (982-7); (C) large, fractured tremolite (grey) grains overgrown by a serpentine (yellowish) mesh, magnetite (black) grains and phlogopite (bluish-green) flakes (982-9); (D) elongated, fractured diopside (light grey) grains, interstitial serpentine (yellowish) and magnetite (black), commonly with iddingsite (brownish), filling gaps between the diopside grains (982-616); (E) magnetite (black) grains and aggregates in serpentine (yellowish) and chlorite (greenish) matrix. Note numerous phlogopite (bluish-green) flakes and bunches (982-10); (F) amphibolite with diopside patches and spots (greenish grey) along the fractures (982-13); (G) olivine-rich zones (black/grey patches) alternate with tremolite-dominant ones (light colored areas). Note iddingsite (olive-green) chains and spots along the zone boundaries and inside the tremolite zone. Black magnetite fills interstices in the olivine-rich zones (D7-3); (H) a contact between actinolite aggregate (greenish, left side) and carbonate (grey, right side). Note euhedral zoned actinolite grains growing at the expense of carbonates (D7-6); (I) serpentine (yellowish) matrix with fine-grained magnetite (dark patches), crosscut by calcite (white) and magnetite (black) veinlets. Note a phlogopite enrichment (bluish green spots on lower left) (D8-2). Scale bar is 1 mm. Plane-polarized light

er with iddingsite and serpentine fill a fracture network (Fig. 4G). A sharp contact of skarn and carbonate rock is observed in **D7-6** (662 m). A fine-grained aggregate of amphibole (mostly actinolite) with diopside relics has a sharp contact with a porous mixture of fine-grained dolomite and calcite (Fig. 4H). The actinolite rock was cross-cut by thin calcite veinlets. Euhedral, zoned actinolite grains grew near the contact, replacing carbonates (Fig. 4H).

The upper part of **D8 cross-section** (Fig. 3C) was drilled through magnetite ores (440–575 m) alternating with serpentinites (e.g. 457–462, 494–498 m) and clinopyroxene-amphibole skarns (e.g. 465–465.8 m), with amphibolite and granite in the middle and lower parts of the core (588–606.5, 700–702 m). Another interval of magnetite ore, skarns and metasomatized amphibolites occurs at 706.8–719 m.

A serpentinite containing magnetite (**D8-2**) was sampled at 490.8 m. A meshwork texture is composed of serpentines, iddingsite, magnetite, and phlogopite bunches and is cross-cut by numerous calcite and magnetite veinlets that commonly contain sulphides (Fig. 4I). Fine-grained magnetite fills the serpentine network, whereas larger grains and aggregates are attached to the veinlets (Fig. 4I). Samples **D8-4** (588 m) and **D8-6** (710 m) are metasomatized alumina-silicate rocks. In D8-4, an oriented, spotted amphibole (hornblende)-plagioclase rock (amphibolite) with presence of biotite and titanite contacts with a predominantly diopside-plagioclase rock. Minor titanite, biotite and K-feldspar are also present. An analcime veinlet cross-cuts the rock. In D8-6, an amphibole plagioclase rock (amphibolite) containing diopside lenses has a contact with an almost monomimerallic hornblende rock. Diopside surrounded by hornblende of varied composition forms the lenses. In **D8-7** from the lower ore interval (714.9 m), layers and lenses of serpentine pseudomorphs with olivine relics, surrounded by magnetite and sulphide aggregates, alternate with tremolite-rich zones with phlogopite flakes, and iddingsite aggregates occur along the different phases.

Mineral compositions and textures

Carbonate. The 982-6 marble consists of granoblastic dolomite crystals with slightly lighter porous areas and alteration zones along grain boundaries and cleavage planes in some places (Fig. 5A). Single olivine (forsterite) grains were replaced by serpentines (Fig. 5B, C). The replacement may have proceeded to completion, leaving behind round aggregates of intermeshed serpentine, commonly with flakes of phlogopite (Fig. 5B). Small porous calcite aggregates occur near cracks or on dolomite grain boundaries (Fig. 5A). Phlogopite flakes tended to form along grain boundaries, cracks or in rounded intergrowths with serpentines (Fig. 5A, B and C). Serpentines also fill and form irregular patches along cracks (Fig. 5B, C). Aggregates of tiny magnetite grains fill interstices along dolomite cleavage planes, and serpentine and phlogopite grains (Fig. 5B, C). Carbonate matrix of 982-4 consists of light gray, slightly zoned calcite grains surrounded by darker gray dolomite (Fig. 8A). Round accumulations of serpentine and iddingsite spot the matrix. Fine-grained magnetite aggregates either impregnated porous carbonate channels or replaced some parts of the rounded serpentine accumulations (Fig. 8B, C). The porous carbonate mixture in D7-6, at the contact with an actinolitic rock, consists of two varieties of dolomite and calcite (Fig. 5D, E). Medium-gray dolomite (1) is surrounded by light-gray calcite and dark-gray dolomite (2), the latter forming thin rims around actinolite grains and porous zones adjacent to those grains (Fig. 6L). Calcite is the major carbonate in the 982-7 brecciated ore (Fig. 5F, G). Highly porous, almost pure calcite grains occur along with tiny dolomite grains along cleavage planes and elongated tremolite grains (Fig. 5F). The carbonate forms layers that alternate with strongly brecciated ore where calcite grains are irregularly shaped and replaced by magnetite along the boundaries in some places (Fig. 5G).

Olivine, orthopyroxene and spinel. Olivine (forsterite) and orthopyroxene (enstatite) –dominant patches occur amongst tremolite-rich zones in the D7-1 and D7-3 samples (Fig. 5H–J). A mesh texture in which serpentine and talc (dark) replace forsterite/enstatite crystals (light gray) along irregular cracks (Fig. 5I, J) is characteristic of these patches. Enstatite has grown at the expense of olivine (Fig. 5I, J). Tremolite, commonly with apatite, and anthophyllite replaces olivine and enstatite (Fig. 5H, J). Olivine relics in dense serpentine mesh were found in the D8-7 serpentine ore (Fig. 5K). Some mesh parts served as pathways for thin magnetite grains to impregnate the rock and to form larger grains. Relics of spinel aggregates, commonly with olivine, are preserved in the carbonate-based (982-3) and serpentine-based (982-10, Fig. 5L) magnetite ores. Irregular cracks in spinel are filled with chlorite and, in places, magnetite films (Fig. 5L).

Clinopyroxene. All clinopyroxenes in the skarns (982-616 and D7-6) and metasomatized alumina-silicate rocks (D8-4, D8-6 and 982-13) are diopside (Table S1). The diopside rock comprising a more than 3 m thick interval (982-616) is spotted by iddingsite, mostly surrounding magnetite and sulphide aggregates (Fig. 6A). Talc pseudomorphs diopside grains in the D7-6 actinolite-rich rock (Fig. 6B). Diopside is a major constituent of diopside-scapolite (±plagioclase) layers, lenses (in D8-4 and D8-6) and patches (982-13) developed in the surrounding alumina-silicate rocks. Such diopside aggregates in the plagioclase/scapolite spotted matrix were in turn replaced by amphiboles, mostly ferropargasite in D8-4 (Fig. 6C) and actinolite in D8-6 (Fig. 6D). Diopside in flattened incontinuous patches (982-13) is porous, and contains scapolite, hornblende and titanite inclusions (Fig. 6E).

Amphibole. The calcic amphibole tremolite is the main mineral in the amphibole-rich zones, alternating with serpentine (±olivine, spinel and/or enstatite) patches in D7-3, D7-1 and 982-11 (Fig. 6F, H) or forming almost monomineralic zones in sample 982-9 (Fig. 6I, J). Anthophyllite is intergrown with tremolite (Fig. 6H) or substituted for enstatite and olivine outside the tremolite-rich zones (Fig. 6F, G). Fractures and intergranular spaces in tremolite grains

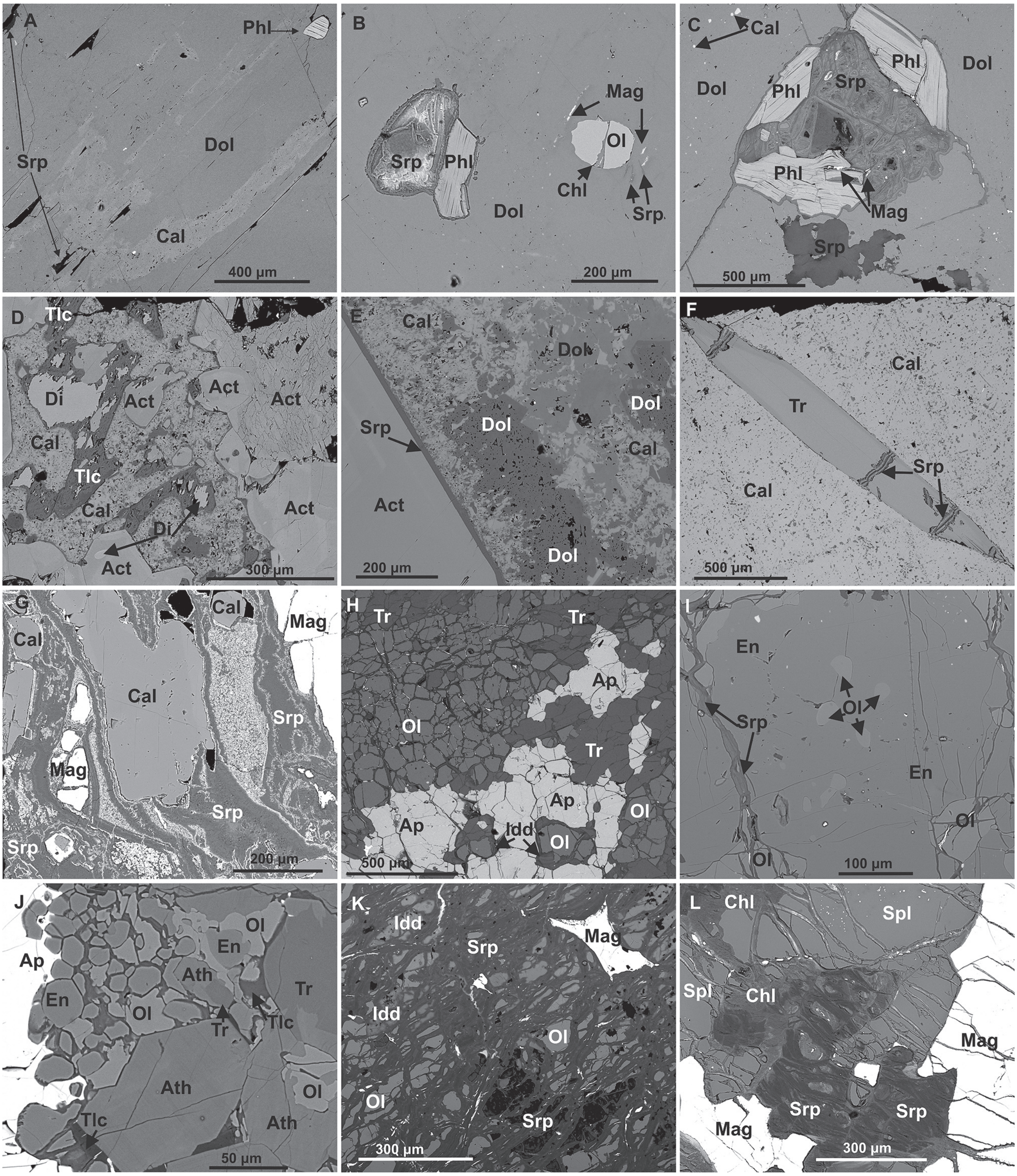

Fig. 5 BSE images of carbonates from 982-6 (A–C), D7-6 (D, E) and 982-7 (F, G); olivine and enstatite from D7-1, D7-3 (H–J) and D8-7 (K); spinel from 982-10 (L). Abbreviations here, in Figs. 2, 3, 6–9 and text are after Kretz (1983). Idd stands for iddingsite, PbTe for lead telluride

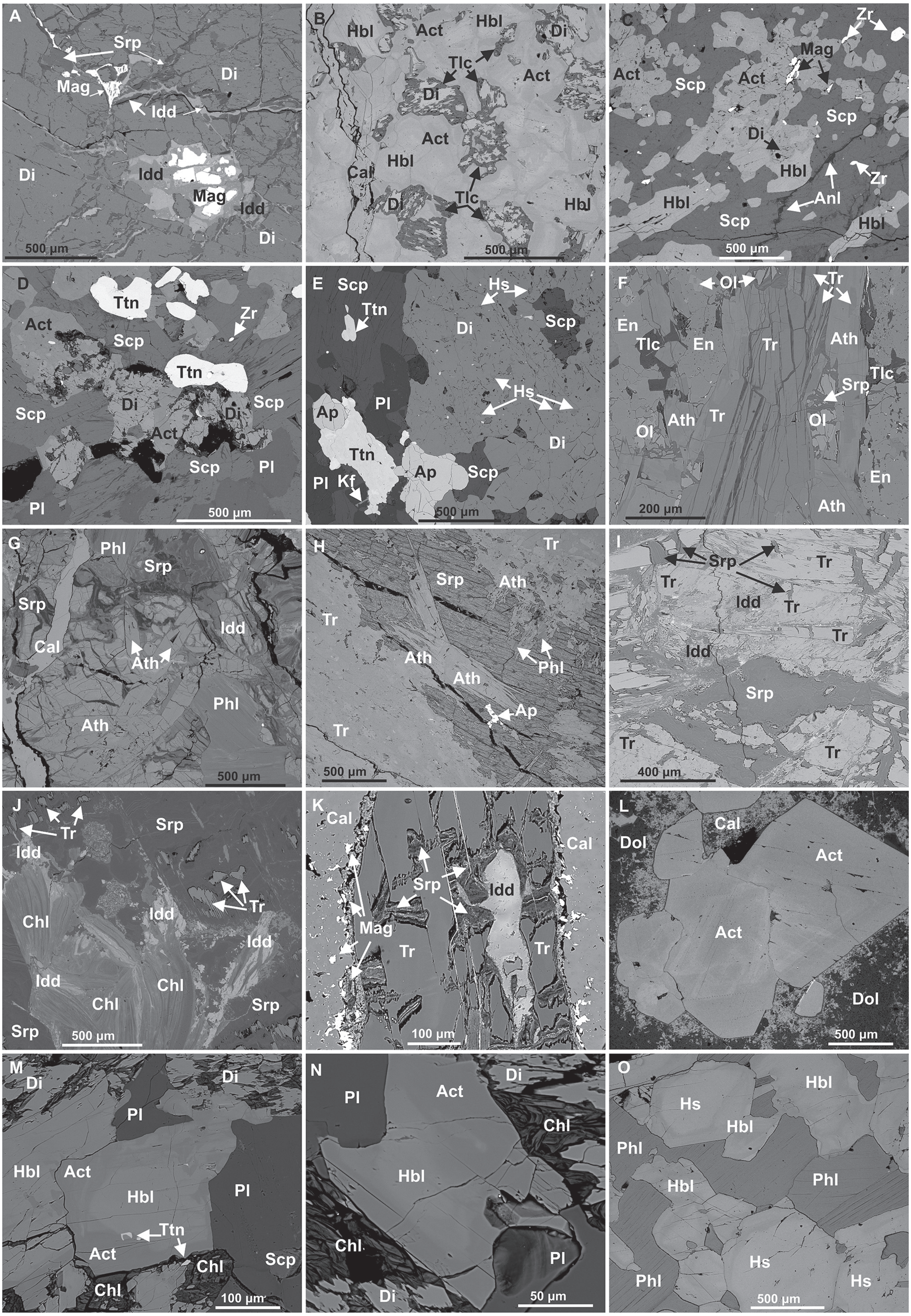

Fig. 6 BSE images of clinopyroxene from 982-616 (A), D7-6 (B), D8-4 (C), D8-6 (D) and 982-13 (E); amphiboles: tremolite from D7-3 (F), 982-11 (H), 982-9 (I, J) and 982-7 (K), anthophyllite from D7-3 (F) and 982-11 (G, H), actinolite from D7-6 (L), D8-6 (M, N), hornblende from D8-6 (M, N) and 982-11

are filled with serpentines in sample 982-9 (Fig. 6I, J), giving way to a mesh of serpentines with magnetite enrichment after the tremolite is almost completely replaced (Fig. 6J). In the brecciated magnetite ore (982-7), cracks in tremolite are filled with serpentines and fine-grained dispersed magnetite (Fig. 6K). Another calcic amphibole, actinolite, replaces diopside in sample D7-6 (Fig. 6B). It is zoned and in places intergrown with hornblende (Fig. 6B). Euhedral actinolite grains grew in the carbonate-rich part of the rock, near the boundary (Fig. 6L). They are zoned, twinned and surrounded by thin dolomite (type 2) rims and "cloudy" calcite (Fig. 6L). Actinolite also substituted for diopside and hornblende in the diopside – scapolite (±plagioclase) rocks, developed in the amphibolites as in the case of the sample D8-6

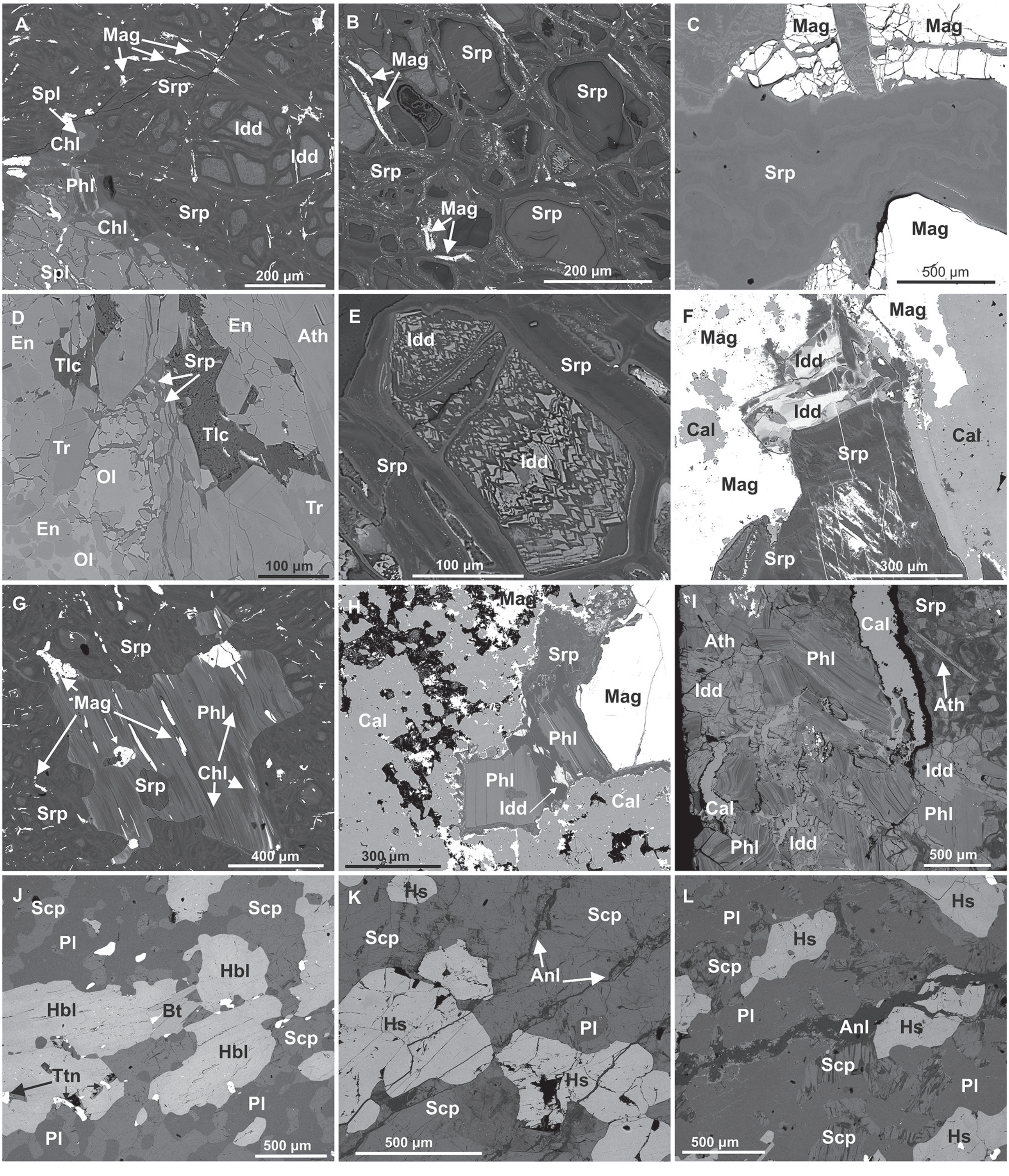

Fig. 7 BSE images of serpentine from 982-10 (A), 982-2 (B), 982-9 (C); talc from D7-1 (D); iddingsite from D8-2 (E) and 982-7 (F); phlogopite from 982-10 (G), 982-7 (H) and 982-11 (I); biotite from D8-4 (J); plagioclase, scapolite and analcime from D8-4 (K, L)

hornblende rock (Fig. 6M). It also replaced primary hornblende in less altered parts of the same sample (Fig. 6N). Magnesiohornblende, pargasite and edenite form transitional zones between serpentine and tremolite skarns (982-11, Fig. 6O) and metasomatized alumina-silicate rocks. Ferropargasite replaces diopsides in some diopside-scapolite zones (e.g. D8-4, Fig. 6C). Edenite and magnesiohastingsite predominated in the less metasomatized parts of amphibolite samples (D8-4, D8-6 and 982-13).

Serpentine, talc and iddingsite. The growth of antigorite at the expense of olivine can be observed in samples of dolomite skarns (982-6), serpentine (D8-2, D8-7, 982-3, 982-9 and 982-10) and brecciated ores (982-7) where it mostly fills mesh interstices (e.g. Fig. 7A, B). Irregular cracks in the mesh- texture are filled mostly with asbestiform varieties of chrysotile and lizardite, in places, tiny flakes of chlorite, calcite, thin-grained magnetite and a non-crystalline, amorphous mixture recognized as iddingsite, as described below (Fig. 7A–F). The round and oval clots in samples 982-3 and 982-4 of carbonate (mostly calcite) skarn (Fig. 4A) are filled with a mixture of asbestiform serpentines and carbonates (serpophite). Fibrous, asbestiform serpentines fill fractures, intragranular spaces or completely replace diopsides and tremolites, as well as formed numerous cross-cutting veinlets (Fig. 7C). Talc is not as abundant as serpentine and mostly replaces diopside in sample D7-6 (Fig. 6B), or enstatite and olivine in samples D7-1 and D7-3 (Fig. 7D).

Along with the serpentines, a mineral or mineral mixture with a higher iron content was recognized in almost all the skarn varieties. It most resembles iddingsite, i.e. a mixture of clay minerals (chlorite group, smectite group), iron oxides and ferrihydrides (Sun 1957; Eggleton 1984; Smith *et al*. 1987), which is commonly derived from alteration of olivine. Since it has a composition that varies from the original olivine through many stages of structural and chemical change, the iddingsite either replaces olivine in distinctive saw-toothed structures (Fig. 7E) or forms irregular patches in the 982-7 ore sample (Fig. 7F) and skarn samples (e.g. D7-1). The highly oxidized iron and ferrihydrides give the rock a brownish, yellowish or greenish hue (Fig. 4D, G, I).

Mica. Single phlogopite flakes and aggregates along fractures occur in the dolomite marble (982-6, Fig. 5A–C). Phlogopite aggregates are most abundant in serpentine-rich parts of the serpentine-based magnetite ores: samples D8-2, D8-7 and 982-10 (Fig. 7G), especially where spinel is present in greater quantities (Fig. 4E). Phlogopite flakes and bunches surround tremolite grains in the brecciated magnetite ore (982-7), or spot the serpentine-enriched parts among tremolitic amphibole (982-11, Fig. 7I). Chlorite flakes or aggregates fill cracks in spinel or replace phlogopite commonly together with magnetite (Fig. 7G). Flakes of primary biotite were preserved along with hornblende in the metasomatized alumina-silicate rocks (e.g. D8-4, Fig. 7J).

Plagioclase and scapolite. Plagioclase in metasomatized amphibolite samples (D8-4, D8-6 and 982-13) are mostly preserved in the least altered rock portions and vary from oligoclase to andesine depending on the whole rock composition (Table S1). Scapolitization is the second most abundant alteration in the alumina-silicate rocks (Fig. 7J-L). Porous and fractured scapolite (light gray) in sample 982-13 of amphibolite replaces plagioclase (oligoclase, dark gray) from grain boundaries toward grain centers (Fig. 7K). Such replacement proceeded to a greater extent in the diopside-scapolite zone of the D8-4 amphibolite where only small round oligoclase grains remain in large scapolite aggregates (Fig. 7J).

Zeolite. Analcime veinlets crosscut the metasomatized amphibolites and fill intragranular spaces and fractures in grains (e.g. D8-4, Fig. 7K, L). Analcime forms relatively large round grains along some fractures in the D8-6 and 982-13 amphibolites. These contain inclusions of K-feldspar, scapolite and calcite. K-feldspathization of plagioclase is a common feature around analcime-filled veinlets and fractures.

Magnetite and sulphide ores

Ores in carbonates

Massive and layered ores. Magnetite mineralization strictly follows the layering of sample 982-3 of spotted carbonate rock (calciphyre) (Fig. 4A). It is possible to observe incipient mineralization phases in the non- mineralized areas of sample 982-4 where minute magnetite grains precipitated in serpentine-filled fractures and porous calcite and dolomite domains at the expense of carbonates (Fig. 8A, B). Monazite also grew in these magnetite-impregnated areas (Fig. 8B). Magnetite- enrichment in the layered parts of sample 982-3 is similar, mostly replacing carbonates and overgrowing larger serpentine and dolomite pseudomorphs (Fig. 8C). That magnetite mostly grew at the expense of calcite is evident in Fig. 8D, where growth along calcite crystal planes did not proceed to completion, leaving behind angular, skeletal magnetite grains. Cracks in some larger aggregates of serpentines and iddingsite are also filled with magnetite (Fig. 8E). Baddeleyite crystals grew together with magnetite in some ore layers in sample 982-3. Some layers (Fig. 4A) preserve small grains of olivine and fractured spinel, as described in the above section.

Brecciated ores. Magnetite behaved differently in the 982-7 brecciated ore where carbonates were intermingled with broken pieces of mesh-serpentine, iddingsite, phlogopite, tremolite grains and aggregates

(Fig. 4B). Minute euhedral magnetites adhere to the boundaries of broken phlogopite, serpentine aggregates (Fig. 8F, G), merging to form solid layers or larger crystals. They also precipitated in pores of carbonates (Fig. 8F). It seems that euhedral magnetite crystals preferred to grow at the expense of calcite, as in Fig. 8F-H. The large magnetite grains display remnants of polygonal texture (Fig. 8F, H, I) and composite growth as described in Prusinskiene *et al.* (2017). Iddingsite mimics euhedral magnetite grain in some places (Fig. 8G). Clots of porous, partly crystallized pyrite with magnetite and titanite pieces occur in the magnetite interstices (Fig. 8I).

Ores in serpentinites (± olivine and spinel)

Several magnetite generations are observed in the 982-10 ore. Magnetite- fills chrysotile interstices in the mesh-textures, forming a complete magnetite web in some places (Fig. 9A). Single euhedral grains fill fractures or pores in spinel grains (Fig. 9A, B). Magnetite grains aligned along chlorite-replacements in the phlogopite flakes (Fig. 7G) or formed euhedral grains when those flakes were completely substituted by chlorite (Fig. 9B). Coarser magnetite grains along spinel or phlogopite grain boundaries are commonly surrounded by skeletal magnetite rims (Fig. 9A–C), indicating multiple stages of magnetite growth. Fine magnetite disseminated along the edges of chrysotile-rich planes and impregnates serpentine-rich parts of the D8-2 ore (Fig. 9C), causing blackening of some yellowish serpentine domains (Fig. 4I). Single magnetite grains comprise parts of the cutting calcite veins. It seems that coarse magnetite grains tended to form together with calcite or replace it (Fig. 9D). The rocks were extensively cross-cut by calcite veins filled not only with magnetite, but also with pyrite, chalcopyrite, sphalerite and other sulphides. As in the above sample, magnetite started to fill chrysotile channels and

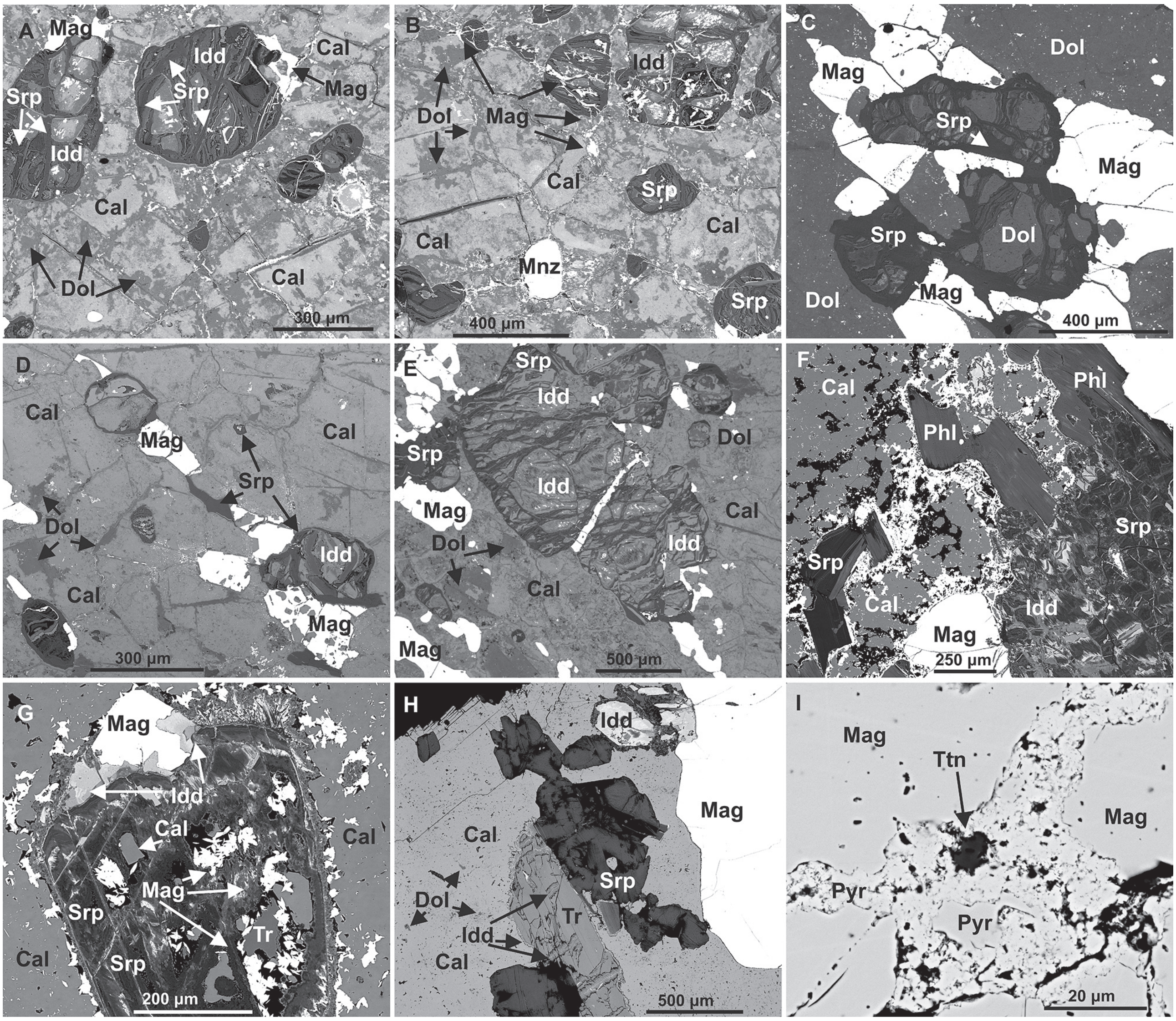

Fig. 8 BSE images of magnetite (A–H) and sulphide (I) ores in carbonates: from 982-4 massive ores (A, B), from 982-3 layered ores (C–E), from 982-7 brecciated ores (F–I).

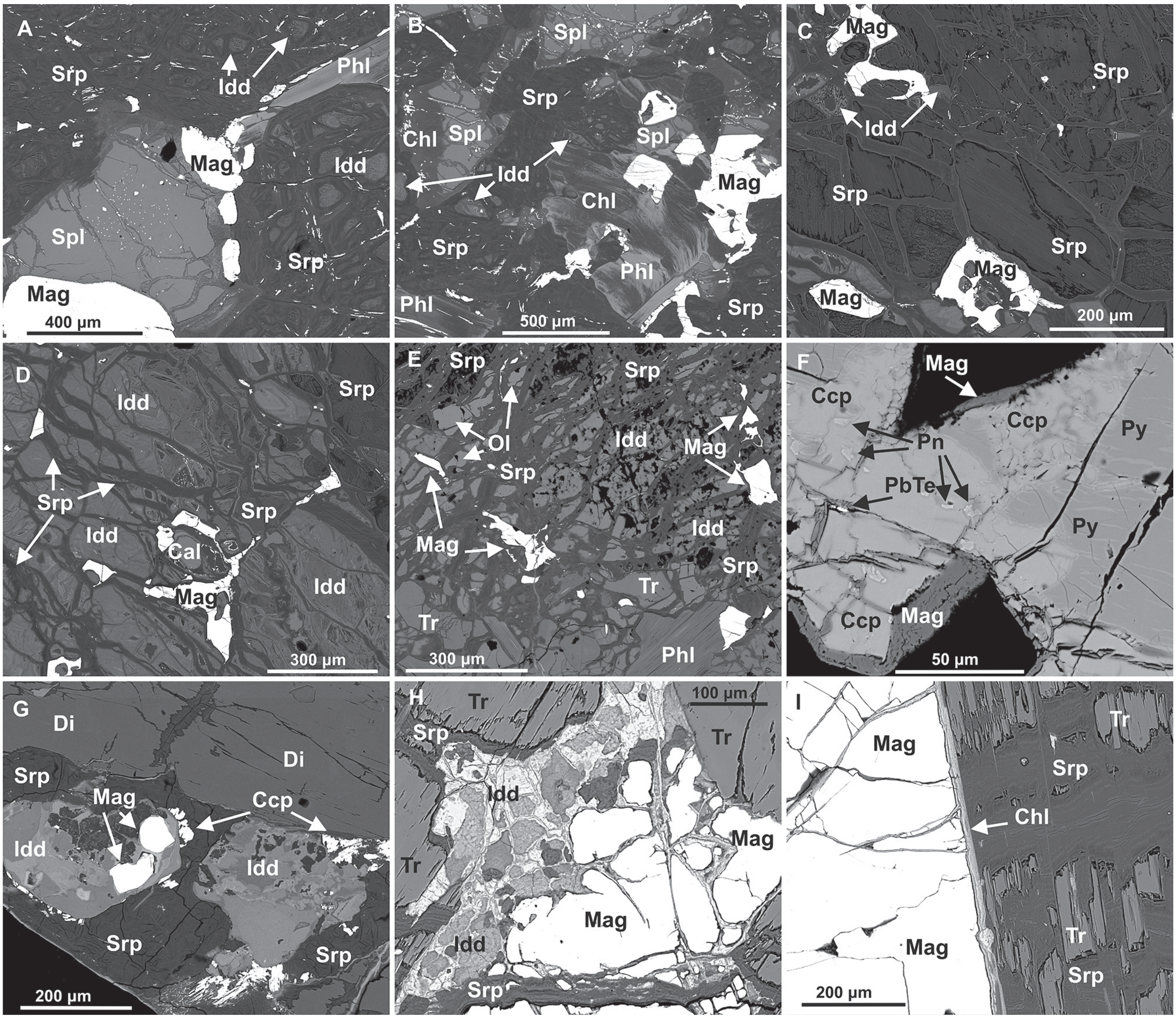

Fig. 9 BSE images of magnetite (A–I), sulphide (F, G) and lead telluride (F) in serpentinites (A–F) from 982-10 (A, B), D8-2 (C, D) and D8-7 (E, F); in diopside rocks from 982-616 (G); and tremolite rocks from 982-9 (H, I)

to grow larger grains in those places in the D8-7 ore (Fig. 9E). Pyrite, chalcopyrite, pentlandite and other sulphides tended to form coarser aggregates around the serpentine-dominated patches (Fig. 9F). Sulphides were overgrown by magnetite rims and have tiny lead telluride (PbTe) inclusions (Fig. 9F).

Ores in diopside rocks

Magnetite is less abundant in the diopside (982-616) and the tremolite-dominated (982-9) intervals. Magnetite either intergrows with iddingsite and fills intragranular spaces between diopside grains (Fig. 9G) or fills fractures and thin films at grain boundaries. Sulphides (chalcopyrite) are apparently later and overgrows the iddingsite replacements (Fig. 9G).

Ores in tremolite rocks

Similarly, as in the diopside rocks, magnetite aggregated into large accumulations in the serpentine-enriched parts of the tremolite rock (982-9, Fig. 9H, I). These accumulations were commonly intergrown with iddingsite and cross-cut by later chrysotile veinlets (Fig. 9H). However, some large magnetite aggregates seem to truncate chrysotile veinlets and have thin chlorite reaction rims (Fig. 9I). Apatite aggregations tended to form together with tremolite as, for example, in the D7-3 tremolite patches in serpentinites (Fig. 5H).

Mineral chemistry

Chemical features of carbonate minerals. Dolomite predominates in the least altered sample of marble (982-6) and is present in the other (mostly calcitic) carbonate-rich samples (982-4, 982-7 and D7-6). All dolomitic marbles have similar calcite (50–53%) and dolomite (41-45%) proportions (Table S1a). Pure dolomite (type 2) surrounds actinolite in sample D7-6 (e.g. Fig. 6L). The dolomites contain up to 3% Fe and

4% Mn in porous or altered parts of the grains (982-6, Table S1a).

The calcite analysed is very pure (98–99% of CaCO$_3$, Table S1a) with MgCO$_3$ up to 11% in sample 982-4, in which calcite is partially replaced by dolomite. The porous matrix carbonate in 982-7 brecciated ore is almost pure calcite (99% CaCO$_3$ with 1% MgCO$_3$) without rhodochrosite and siderite end members (Table 1a), whereas calcite in the ore-enriched part contains slightly more Mn- and Fe (1% MnCO$_3$ and 0.5% FeCO$_3$). The dolomite clots in porous calcite contain up to 3% MnCO$_3$ and 2% FeCO$_3$.

Chemical characteristics of the forsterite, enstatite and spinel mineralization. All olivine is forsterite (Table S1b), with Mg/(Mg-Fe) number mostly of 83-84%, reaching 89% only in the dolomite marble (982-6). Forsterite grains are nearly with Mn and Ca not exceeding 0.23 wt% (Table S1b). The enstatite replacing olivine has a very similar Mg# (Table S1c). The Mg# in spinel is lower (66–67%). Spinel grains in the magnetite ore (982-10) are slightly enriched in ZnO (0.35 wt%, Table S1b).

Chemical features of the diopsides. The diopsides can be divided into two groups (Fig. 10). Diopsides in the skarns (982-616 and D7-6) differ from those in the metasomatized alumina-silicate rocks (D8-4, D8-6 and 982-13) in their higher Mg# (0.85–0.95) and lower alumina (depicted as atoms per formula unit in Fig. 10) content (Table S1c). Diopsides from the 982-616 rock have the lowest diopside FeO content (2.6 wt%), lower than in the diopside relics of the D7-6 skarn (5.5 wt%) and no alumina at all (Fig. 10). Some diopside relics in actinolite rock (D7-6) are Fe-enriched, causing those spots to plot in the Mg# vs Al per formula unit diagram in the lower field together with those from the metasomatites (Fig. 10). Diopsides from the diopside-scapolite portion of the metasomatized amphibolite (D8-4) have the highest Al (up to 1.62 wt%) and FeO (12.42 wt%) contents (lower right, Fig. 10).

Chemical features of the amphiboles. Magnesium (iron and manganese)- amphibole anthophyllite (Fig. 11A) formed mostly in the skarns and replaced olivines, enstatites and tremolites. Among the amphiboles, it has the lowest calcium (0.48–1.39 wt%), the highest magnesium (reaching 27.64 wt%) contents and no alumina (Table S1d).

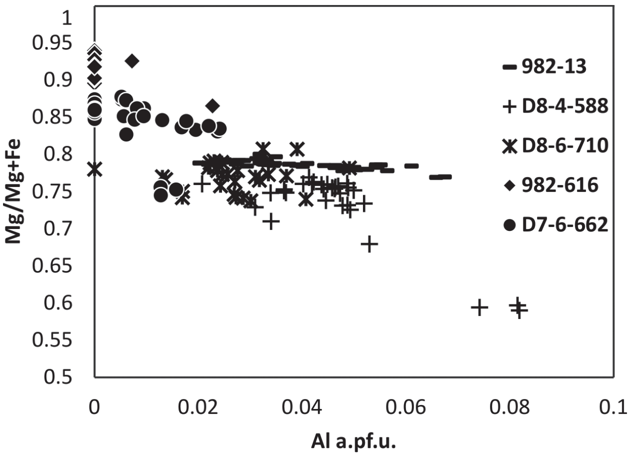

Fig. 10 A Mg# *vs* Al per formula unit diagram for clinopyroxenes

The calcic amphibole is tremolite, whether forming thick zones (982-9) and patches among serpentine-rich rocks (D7-1, D7-3, 982-11) or ores (D8-7 and 982-7), or replacing the diopside (982-616), has a narrow range of composition, with MgO (26–27 wt%), CaO (10–12 wt%) and FeO (ca. 3 wt%, Table S1d). The Mg# varies around one and they plot in a narrow field in the amphibole classification diagram after Leake *et al.* (1997) (Fig. 11B). Actinolite in the actinolite-rich rock (replacing diopside) and from the contact zone with carbonates (D7-6) has higher iron (ca. 9 wt%), lower magnesium (down to 18 wt%) and up to 2 wt% of alumina (Fig. 11B, Table S1d). Some zones in those actinolites are enriched in alumina (4 wt%), iron (11 wt%) and sodium (1.6 wt%) and thus plot in the magnesiohornblende field (Fig. 11B). The actinolite, replacing diopside in the metasomatized amphibolite (982-13), does not differ except for slightly higher iron (to 11 wt%) and alumina (to 3 wt%, Table S1e) contents.

In sample 982-11, the hornblendite zone is made of magnesiohornblende (richer in Fe, Fig. 11B), which is adjoined by the almost pure pargasite/edenite rock at the contact with the metasomatized amphibolite (Fig. 3C). The pargasite/edenite (982-11) resembles amphiboles from the amphibolite in their alumina and sodium contents (App., Table 1e, Fig. 11B) and differs only in their higher MgO content (up to 18 wt%).

In the metasomatized amphibolites (D8-4, D8-6 and 982-13), the majority of amphiboles plot in the magnesiohastingsite and edenite fields (Fig. 11C). Some ferropargasites (Fe-enrichment to 21wt% at the expense of Mg, Table S1, Fig. 11C) occur as inclusions in or intergrowths with diopside in the diopside-scapolite-rich part of sample D8-4 (Fig. 11C). Some edenites from the least altered amphibole-plagioclase (±scapolite) parts (Fig. 11C) have the highest TiO$_2$ amongst the amphiboles (to 1.26 wt%), are rich in Na$_2$O (2.21wt%) and Al$_2$O$_3$ (ca. 10 wt%) contents (Table S1e).

Chemical features of serpentines and iddingsite. The serpentines differ in their iron and magnesium contents (Table S1f). Light gray antigorite pseudomorphs after olivine in the meshy serpentine matrix of the magnetite ores (D8-2, D8-7 and 982-10) have very similar SiO$_2$ (ca. 39 wt%), but variable FeO (12–20 wt%) and MgO (27–35 wt%) contents. Mg# varies from 0.72 to 0.84. The irregular frac-

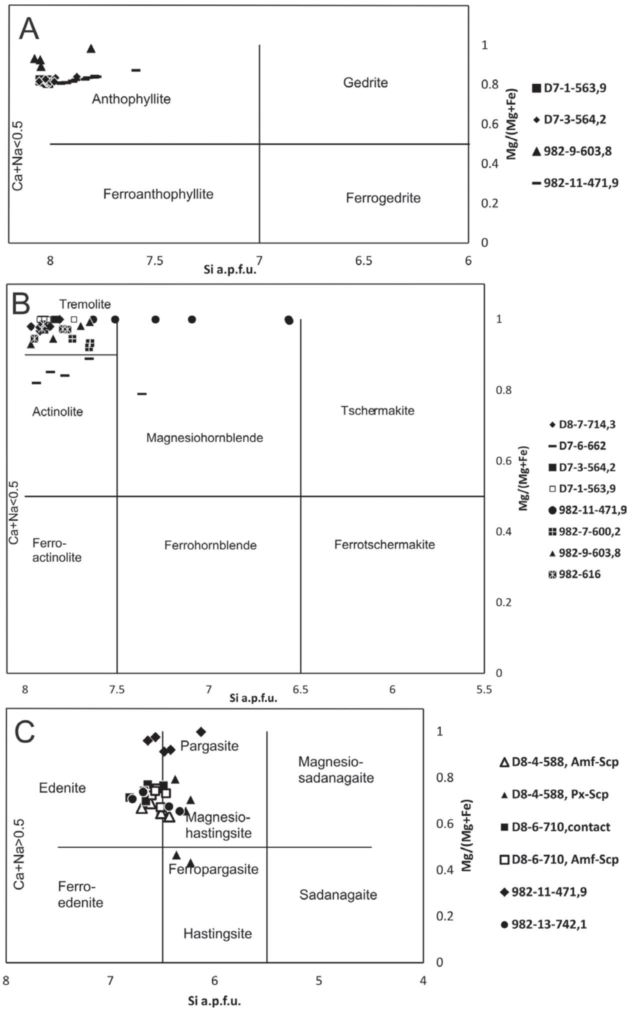

Fig. 11 Amphibole classification diagram: for magnesium (iron and manganese)- amphiboles with diagram parameters: $(Ca + Na_B) < 1.00$, $(Mg, Fe^{2+}, Mn, Li)_B \geq 1.00$, $Li_B < 1.00$ (A); calcic amphiboles with diagram parameters: $Ca_B \geq 1.50$, $(Na + K)_A < 0.50$ (B); calcic amphiboles with diagram parameters: $Ca_B \geq 1.50$, $(Na + K)_A \geq 0.50$ (C) after Leake *et al.* (1997)

tures in the carbonate skarn (982-4, Fig. 9A, B) are filled mostly with lizardite and chrysotile. The lizardite has variable iron (5–14wt%) and magnesium (32–39wt%) contents, while the asbestiform chrysotile is the most Mg-rich (41–42 wt%) and Fe-poor (2–3.3 wt%, Table S1f). Its Mg# reaches 0.97. The layered, asbestiform chrysotile in the veinlet cross-cutting the tremolite rock (982–9) has up to 1.12 wt% of alumina.

The iddingsite can be distinguished from serpentine by its elevated and variable iron content (12–40 wt%, Table S1g). The content of SiO_2 varies from 32 to 49 wt%, MgO from 11 to 32 wt% (Table S1g). No mineral formula can be calculated because iddingsite is a polyphase aggregate rather than a single mineral (cf. Smith *et al.* 1987).

Chemical features of micas. The phlogopite flakes in the dolomite marble (982-6, Fig. 5A) are Fe-poor (3.5 wt%, Table S1h), Mg-rich (26 wt%) and contain up to 0.5 wt% fluorine. The bunches of phlogopite flakes in the serpentine-dominated patches among tremolites (982-9 and 982-11), serpentine-based magnetite (D8-2, D8-7 and 982-10) and brecciated ores (982-7) have similar FeO (4-5 wt%) and MgO (24–26 wt%) contents, but higher (up to 20 wt%) Al_2O_3 content in the spinel-enriched parts (982-10, Fig. 5L), or contain up to 1 wt% of Na_2O near contacts with alumina-silicate rocks (982-10 and 982-11, Table S1h). Biotite relics in both the diopside-scapolite-dominant or less altered amphibolite parts (D8-4, D8-6 and 982-13, Fig. 7J) have similar chemical compositions (ca. 12 wt% of FeO and ca. 18 wt% of MgO) with high TiO_2 (1.8-2.7 wt%, Table S1h).

Chemical features of plagioclase and scapolite. Plagioclases in sample D8-4 are commonly andesines with anorthite content varying from 25 to 29% (Table S1i). They are oligoclases (An_{20}) in relics amongst scapolites in sample D8-4 (Fig. 7K). In contrast, plagioclase is richer in Ca (An_{30-33}) at the boundaries with Mg-enriched amphiboles. The anorthite equivalent in the scapolites varies from 30 to 40% and, thus, shows Ca-enrichment. Oligoclase predominates in the altered D8-6 (An_{13-25}, Table S1i) and 982-13 (An_{19-24}) amphibolites. Some albite grains are found near quartz and K-feldspar aggregates in the more felsic D8-6 rock (Table S1i). The anorthite equivalent in the scapolites varies from 27 to 33%.

Magnetite compositions. Four magnetite generations were recognized in the earlier studied D8 serpentine-based ores (Prusinskiene *et al.* 2017). All the magnetites have similar TiO_2 (0.2–0.4 wt%) and V_2O_3 (from 0 to 0.4 wt%) contents but differ mostly in alumina (from 0 to 1 wt% of Al_2O_3), with Ca+Al+Mn varying from 0.03 to 0.3 (Table S1j). In Ti + V *vs* Ca + Al + Mn magnetite discrimination diagram by Dupuis, Beaudoin (2011), they plot in the Kiruna or Porphyry type fields (Fig. 12A). The newly studied magnetites from the serpentine-based (982-10) and tremolite-based (982-9) ores have rather constant Al_2O_3 contents (average 0.3–0.4 wt%, up to 2 wt%), but lower TiO_2 and V_2O_3 contents not exceeding 0.1 wt% in most samples (Table S1j). Therefore, the vast majority of magnetites plot in the iron oxide- copper- gold (IOCG) and Skarn fields with a few samples located in the BIF area (Fig. 12A).

The most inclusion-free 982-9 magnetites are richer in Fe than the 982-10 magnetites which have higher alumina and magnesium contents as it is shown in the Fe *vs* Ca + Mg + Al + Si diagram after Hu *et al.* (2014) used for magnetite discrimination (Fig. 12B). To sum up, the magnetites (especially from the 982 drill-core) are low in Ti, V, Mn and feature Mg and Al mineral inclusions in some places. Other ores, such as apatite and pyrite are enriched in fluorine.

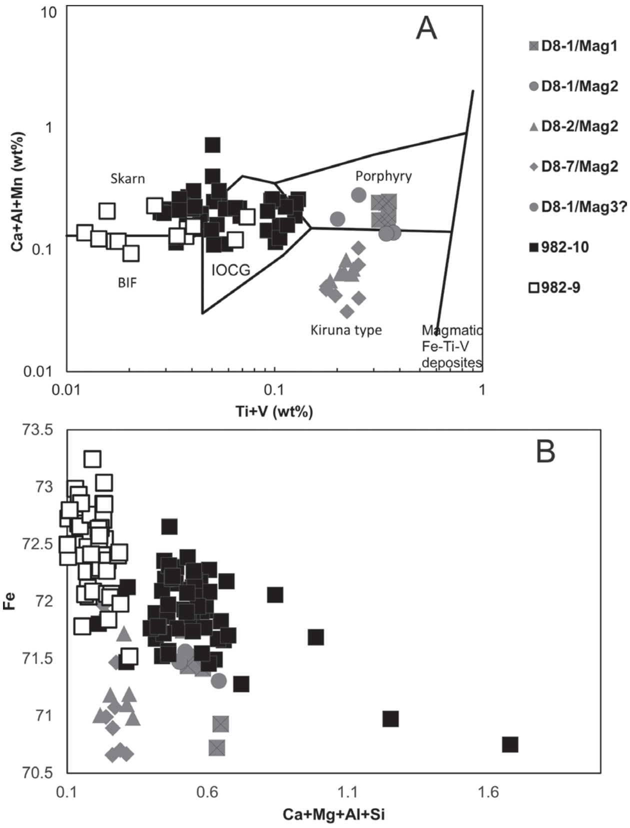

Fig. 12 Ti + V *vs* Ca + Al + Mn magnetite discrimination diagram (A) by Dupuis, Beaudoin (2011). Chemical analyses of Mag from the D8-1, D8-2 and D8-7 skarns (grey symbols) from Prusinskiene *et al.* (2017) have been plotted for comparison. Fe *vs* Ca + Mg + Al + Si diagram (B) after Hu *et al.* (2014) used for magnetite discrimination. Note the gradually decreasing Ca + Mg + Al + Si and increasing Fe content in the analyzed data away from the primary magnetite field (coming from granite source according to Hu *et al.* (2014)), implying gradual removal of silicates and their replacement by iron

Monazite ages

Monazites are quite rare in the study rocks. They are most abundant in the 982-4 calciphyre, but only in a narrow zone together with incipient magnetite mineralization (Fig. 8B). The grains are mostly distributed along calcite grain boundaries and are rimmed by dolomite (Fig. 8B). In some cases, small magnetite grains accumulated along monazite grain boundaries (Fig. 8B). The monazites are from 20 µm to 250 µm long. The largest grains are mostly euhedral or subhedral and fractured in most cases (Fig. 13A). They display clear zoning patterns in BSE images, with dark cores irregularly overgrown by brighter rims (Fig. 13A). The cores are commonly richer in Th and Y than the rims (Table S2). In the cores, the Th is higher than 2 wt%, except for the darkest patches, whereas in rims it varies from 0.95 to 2.13 wt%. The rims are slightly richer in LREEs than the cores. The smallest grains are more irregularly shaped, but better preserved (Fig. 13A). They appear homogeneous in the BSE images and have chemical compositions like that of the rims of the larger grains (Fig. 13A, Table S2). All the monazite grains have U content below detection limit of Cameca EPMA (95 ppm), thus the age was calculated using the Montel equation (Montel *et al*. 1996).

The monazite EPMA spot ages are scattered (Table S2), but the oldest apparent ages (from 4.3 to 1.8 Ga) have very high errors and very low Th contents and were dismissed from estimates. The remaining single point ages ranging from 1.87 Ga to 1.41 Ga can be subdivided into two groups based on chemical composition and location within the grain. A weighted average age of 1536 ± 82 Ma (n = 14. MSWD = 0.15) was calculated from the bright BSE rims and the smallest homogeneous grains (Fig. 13B). A weighted average age of 1781 ± 60 Ma (n = 12, MSWD = 0.077) recorded by the core of the best-preserved large grain number 1 (Fig. 13C) is very similar to a weighted average age of 1774 ± 45 Ma (n = 23, MSWD = 0.17, Fig. 13D), which was yielded by the monazite cores.

DISCUSSION

The study of detailed textural and mineral compositions of the VIOZ rocks provides an opportunity to shed light on the origin and evolution of the skarns and metasomatites. Progressive skarn development in the dolostones and subsequent alteration of the alumina-silicate rocks (amphibolites and gneisses), ore mineralization, the timing of some skarn groups and regional implications will be discussed.

Skarn and metasomatite formation. The rocks can be subdivided into several groups according to their stage-by-stage evolution: 1) high-grade skarns (containing forsterite, enstatite, spinel and diopside) and metasomatites (containing diopside); 2) medium-grade skarns (containing tremolite, actinolite, anthophyllite, hornblende, phlogopite and apatite) and metasomatites (containing hornblende, biotite, feldspar and scapolite); 3) low-grade skarns (containing serpentine, iddingsite, chlorite, zeolites, magnetite and sulphides).

1) The dolomite and impurities were metamorphosed to dolomite marble, forsterite (silica-rich domains) and spinel (alumina-rich domains) rocks during regional metamorphism. The metamorphism triggered CO_2 and H_2O circulation, leading to the formation of extensive forsterite (± enstatite and spinel) and diopside zones. According to previous P-T investigations (Skridlaite 1993a) and the metamorphic grade of the host rocks, the metamorphism and metasomatism probably proceeded in a closed-system of fluid circulation. Talc and tremolite relics among the forsterite, tremolite and enstatite grains in the D7-1

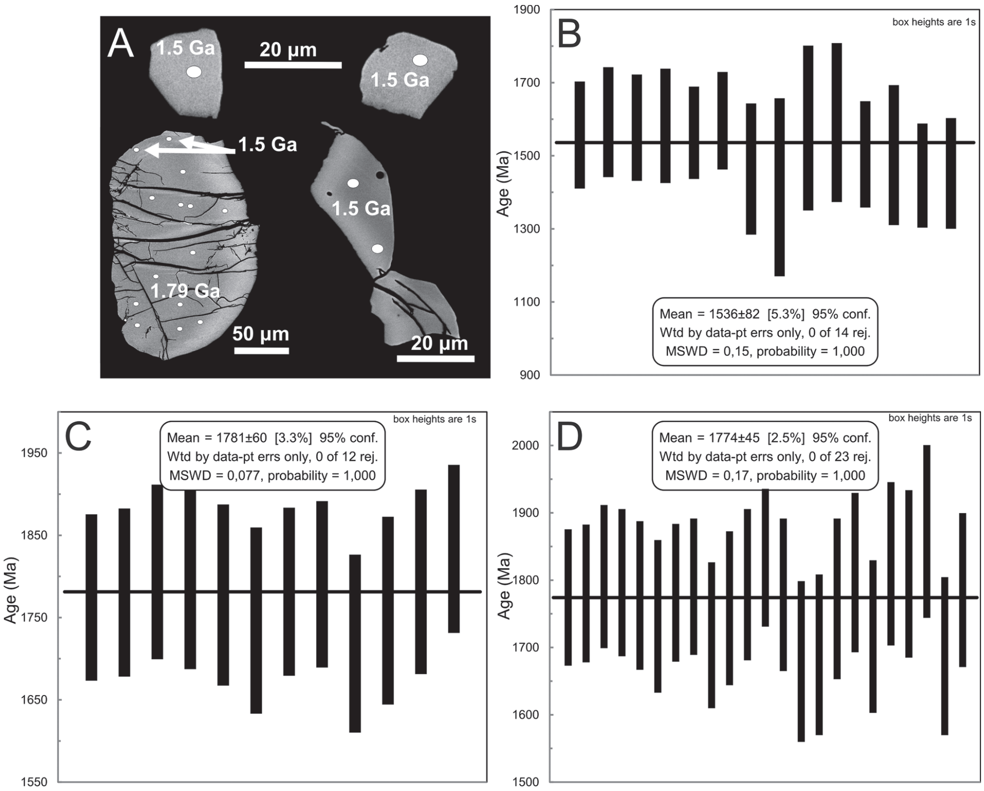

Fig. 13 The 982-4 monazite age data: BSE images of the representative monazites (A); a weighted average age calculated from: the bright BSE rims and the smallest homogeneous grains (B), the best-preserved large grain number 1 (C), the monazite cores (D)

(Fig. 7D), may be evidence of the prograde reactions (1): 3Dol + 4Qtz + H_2O = Tlc + 3Cal + $3CO_2$ (Gordon, Greenwood 1970) and (2): 5Tlc + 4Qtz + 6Cal = 3Tr + $6CO_2$ + $2H_2O$ (Metz *et al.* 1968). As temperature increased further (up to ca. 700° C at 5–6 kbar, Bowen 1940), forsterite has appeared via the reaction (3): 11Dol + Tr = 8Fo + 13Cal + H_2O + $9CO_2$. Similar maximum temperatures for skarn formation were proposed by Skridlaite (1993a). In places of local SiO_2 enrichment, enstatite was likely produced instead of forsterite, as it is mostly associated with forsterite (Fig. 5I, J). Since spinel is the usual Al-rich phase at higher pressures (Widmark 1980) in the upper amphibolite facies, it might have developed in alumina-enriched zones (Fig. 5L) subsequently (or coevally??) with forsterite.

The reaction (4): Cal + Tr = Dol + 4Di + H_2O + CO_2 may have introduced diopside into the impure dolostone system if the fluid was CO_2 rich (X_{CO2} > 0.7, Dachs, Metz 1988). The appearance of diopside zones may also depend on bulk rock composition (high-SiO_2-low-Mg/Fe carbonates) or considerable SiO_2-enrichment during infiltration vs diffusion. The latter explanation may account for diopside zones in the 982, D7 and D8 core-sections because they usually occur at the carbonate body margins (Fig. 3A–C) and were subject to SiO_2 infiltration/diffusion from the felsic host rocks. Diopside patches, veinlets, lenses and layers in the alumina-silicate rocks (mostly amphibolites and gneisses) were produced at the expense of hornblende (magnesiohastingsite or edenite), biotite and plagioclase (Fig. 6C, D). Ca-enrichment is prominent in those zones.

The fact that no wollastonite was found in the rocks may be evidence that no temperatures higher than 750^o C were attained. Similar peak temperatures of 700-750^o C in the VIOD (obtained by geothermobarometric calculations and temperature estimations using fluid in quartz and calcite inclusions) were reported by Skridlaite (1993a).

All the above reactions release water and volatiles and need a considerable amount of SiO_2 which was hardly present in the carbonate rocks in such quantity. Infiltration vs diffusion -driven metasomatism was responsible for Mg leaching from dolomites and Mg and -Si enrichment in the forsterite zone. Enstatite appeared instead of/after forsterite together with local Si-enrichment. Ca moved out of the dolomites, partly accumulating in the outer diopside zone. Ca and Mg were responsible for large-scale metasomatism in the neighboring alumina-silicate rocks (mostly amphibolites) leading to extensive diopside and later scapolite zones.

2) After the rocks have reached their T maximum (at ca. 700–750° C), they were uplifted. At lower pressures, anthophyllite (stable below 650° C and

6.5 kbar) was introduced into the system at the expense of enstatite (5): $9En + 2H_2O = 2Ath + 2Fo$, as can be observed in Figs. 5J, 6F–H. With decreasing T, tremolite replaced diopside via reaction (4), or diopside and enstatite via reaction (6): $3En + 5Di + 2H_2O + 2CO_2 = Dol + 2Tr$, or forsterite and diopside (7): $2Fo + 11Di + 3H_2O + 5CO_2 = 3Tr + 5Cal$ etc. Apatite grains and aggregations commonly accompanied the tremolite replacement (e.g. D7-1, Fig. 5H). More Fe- and Al-rich actinolite (Fig. 5D, E), has appeared instead of tremolite in the outer skarn body zones close to the amphibolites and gneisses. Phlogopite commonly replaced spinel, however an increase in phlogopite aggregations (e.g. 982-10, Fig. 4E) near the contact with host rocks may indicate a diffusion of Al_2O_3 from the host rocks (amphibolites and gneisses).

3) When the higher-grade skarns and metasomatites were exposed to lower temperatures and hydrous conditions, they were replaced by variable serpentines, iddingsite, talc, chlorite and even zeolites. Fluid influx has increased rock volume, leading to intensive fracturing and veinlet formation. The antigorite pseudomorphs after olivine in serpentine mesh hollows (e.g. Fig. 7A, B), surrounded by irregular cracks filled mostly with asbestiform varieties of chrysotile and lizardite, chlorite, calcite, thin-grained magnetite and iddingsite (Fig. 7A–F) have completely replaced the forsterite skarns in many places. Talc and fibrous, asbestiform serpentine zones appeared at the expense of diopside and tremolite ones (Fig. 9I). The rocks were crosscut by numerous asbestiform serpentine (Figs. 6I, 7C) and calcite (6G) veinlets. Chlorite has replaced spinel (Fig. 5L) and phlogopite (Figs. 7G and 9B).

Ore formation. According to recent observations, magnetite in great quantities was not formed until later stages of metamorphism when iron was brought by water-rich fluids and precipitated in former carbonates and skarns, mostly fractures and veins. It seems that iron replaced some magnesium in serpentinites (Fig. 8C) but the process was rather limited. Several details, such as magnetite crystal growth together with chlorite (Figs. 7G, 9B), iddingsite and magnetite intergrowths (e.g. iddingsite precipitation mimicking a magnetite grain after the magnetite stopped growing in Fig. 8G), fracture filling by tiny magnetite aggregates (cf. Figs. 8A, B, 9A and B), skeletal carbonate replacement (Fig. 8D), magnetite precipitation in porous calcite (Figs. 7H, 8F and G) etc., point toward late stage magnetite and subsequent or slightly later sulphide mineralization. According to textural relationships and chemical characteristics, magnetites of at least four types were recognized (Prusinskiene *et al*. 2017). In this study, magnetites from two samples plot in the skarn and iron oxide-copper-gold (IOCG) fields (Fig. 12A). The fact that magnetite plots in the different origin ore fields (Fig. 12A; Prusinskiene *et al*. 2017), may indicate that iron came from different sources rather than a uniform source.

To sum up, the studied zones distinguished in the studied rocks: forsterite (± enstatite and spinel) – diopside – tremolite (± actinolite, pargasite, hastingsite, phlogopite, apatite, scapolite) – talc (± serpentine, iddingsite, chlorite, magnetite, sulphides, zeolites), are quite complex, but their fragments described in Korzhinskii (1970), Meinert (1992, 1997), Zharikov, Rusinov (2015) etc.

Age of metasomatism and implications for regional evolution. Relics of ca. 1.89 Ga metamorphosed diorite-granodiorite-granite suite (Siliauskas *et al*. 2018b) are present beneath the VIOD skarns and metasomatites in some drillings. The VIOD is hosted by an apparently younger metamorphosed sedimentary – volcanic complex that might have formed semi-simultaneously with ca. 1.83 Ga Lazdijai volcanic complex further west (Siliauskas *et al*. 2018a). An accretion-related regional metamorphism of ca. 1.80 Ga was recorded in the area, accompanied by ca. 1.79 Ga gabbro-norite intrusions (Bogdanova *et al*. 2015). The 1.77 –1.78 Ga ages yielded by the 982-4 monazite cores may relate the high-grade skarn formation to the ca. 1.79–1.80 Ga regional metamorphism. Later shearing and metamorphic overprint of ca. 1.71–1.66 Ga (Bogdanova *et al*. 2001) as well as zircon resetting at 1.73 Ga (Siliauskas *et al*. 2018a) were prominent in the region and, likely, contributed to the later skarn formation and ore mineralizations. A ca. 1.54 Ga age recorded by the 982-4 monazite rims and small homogeneous grains is in a good agreement with the ca. 1.53 Ga age of the Druksiai–Polotsk Deformation Zone further north (Vejelyte *et al*. 2010). It is simultaneous with the 1.55–1.50 Ga Mazury AMCG complex and Kabeliai intrusions (cf. Skridlaite *et al*. 2003, 2006, Sundblad *et al*. 1994) to the south, which are rich in fluids, iron, REE and other components. Thus, the ca. 1.54 Ga age may be considered as the late ore mineralization phase.

CONCLUSIONS

The combined study of rock textures in BSE images and mineral chemistry allowed to reconstruct several episodes of skarn and metasomatite formation in the concealed Proterozoic basement of Lithuania, within the Varena Iron Ore deposit (VIOD).

High-grade skarns (700–750° C and 5–6 kbar) started to form in carbonate rocks where SiO_2 content was enough for forsterite or enstatite (instead of/after forsterite together with local Si-enrichment) formation. Spinel appeared in places of a local Al-enrichment. Released water and CO_2 have facilitated an extensive metasomatism and skarn zone formation. Monazite cores in the calciphyre were dated at ca. 1.78 Ga which is the age of regional metamorphism in the area.

During the subsequent uplift and retrogression, influx of water rich fluid facilitated an extensive formation of hydrous minerals. Phases such as tremolite, actinolite, anthophyllite, hornblende, phlogopite and apatite overprinted the preexisting skarn zonation, and in places formed monomineralic zones.

The low-temperature water fluid-influx caused a voluminous serpentinization, iddingsite and chlorite formation as well as brought iron, sulphides, and other mineralizations. Small homogeneous monazite grains and rims in the studied calciphyre yielded ca. 1.54 Ga, coinciding with the emplacement of voluminous AMCG suites such as the Mazury complex and the Kabeliai intrusions further south. To establish a relationship between the abundant sulphide, iron oxide and REE mineralizations in the Mazurys complex and in the VIOD would enhance considerably a potential of mineral resources in the whole region.

ACKNOWLEDGEMENTS

The research of Siliauskas and Prusinskiene was supported by the Nature Research Centre doctoral study funds. The authors are grateful to Lidia Jeżak and Petras Jokubauskas from the EPMA laboratory at Warsaw University for assistance with monazite dating. We also thank Prof. Ray Macdonald for the language corrections. Daniel Dunkley and Ewa Krzeminska are highly appreciated for valuable corrections and comments which helped to improve the manuscript.

REFERENCES

Bogdanova, S.V., Page, L.M., Skridlaite, G., Taran, L.N. 2001. Proterozoic tectonothermal history in the western part of the East European Craton: $^{40}Ar/^{39}Ar$ geochronological constraints. *Tectonophysics 339 (1–2)*, 39–66.

Bogdanova, S., Gorbatschev, R., Skridlaite, G., Soesoo, A., Taran, L., Kurlovich, D. 2015. Trans-Baltic Palaeoproterozoic correlations towards the reconstruction of supercontinent Columbia/Nuna. *Precambrian Research 259*, 5–33.

Bowen, N. L. 1940. Progressive metamorphism of siliceous limestone and dolomite. *Journal of Geology 48*, 225–274.

Dachs, E., Metz, P. 1988. The mechanism of the reaction 1tremolite + 3calcite + 2quartz = 5 diopside + $3CO_2$ + $1H_2O$: results of powder experiments. *Contributions to Mineralology and Petrology 100*, 542–551.

Dupuis, C., Beaudoin, G. 2011. Discriminant diagrams for iron oxide trace element fingerprinting of mineral deposit types. *Mineral Deposita 46*, 319–335.

Eggleton, R.A. 1984. Formation of Iddingsite Rims on Olivine: A Transmission Electron Microscope Study. *Clays and Clay Minerals 32 (1),* 1–11.

Gordon, T.M., Greenwood, H.J. 1970. The reaction: dolomite + quartz + water = talc+ calcite + carbon dioxide. *American Journal of Science 26*, 225–242.

Hu, H., Li, J.L., Lentz, D., Ren, Z., Zhao, X.F., Deng, X.D., Hall, D. 2014. Dissolution-reprecipitation process of magnetite from Chengchao iron deposit: Insights into ore genesis and implication for in-situ chemical analysis of magnetite. *Ore Geology Reviews 57*, 393–405.

Kepežinskas, K., Šliaupa, S. 1994. Varėna iron ore deposit – the part of layered magmatic chamber. In: Kadūnas, V. (ed.), *Problems of bedrock research, utilization and protection in Lithuania*. Geologijos institutas, Vilnius, 58–59 [In Lithuanian].

Kirkliauskaite, V., Motuza, G., Skipityte R. 2016. Varėna Suite in the Crystalline Crust of the Southern Lithuania: Implication to the Genesis and Mineralization.

Klein, V.M., Puura, V.A., Birkis, A.P., Kopelmaa, Ch.J., Motuza, G.B., Skridlaite, G.V. 1990. Metamorphism of the Precambrian complexes in Baltic countries. In: *Precambrian Geology and Geochronology of the East European Platform*, 146. Leningrad [In Russian].

Korzhinskii, D.S. 1970. *Theory of Metasomatic Zoning*. Oxford, UK: Clarendon Press.

Kretz, R. 1983. Symbols for rock-forming minerals. *American Mineralogist 68*, 277–279.

Leake, B., Woolley, A.R., Arps, C.E.S., Birch, W., Gilbert, M.C., Grice, J D., Hawthorne, F.C., Kato, A., Kisch, H.J., Krivovichev, V.G., Linthout, K., Laird, J., Mandarino, J.A., Maresch, W., Nickel, E.H., Rock, N.M.S., Schumacher, J.C., Smith, D.C., Stephenson, N.C.N., Ungaretti, L., Whittaker, E.J.W., Youzhi, G. 1997. Nomenclature of amphiboles: report of the subcommittee on amphiboles of the international mineralogical association, commission on new minerals and mineral names. *The Canadian Mineralogist 35*, 219–246.

Ludwig, K.R. 2012. Isoplot 3.75. A geochronological toolkit for microsoft excel. *Berkeley Geochronology Center, Spec. Pub. 5*.

Mansfeld, J. 2001. Age and εNd constraints on the Palaeoproterozoic tectonic evolution in the Baltic-Sea region. *Tectonophysics 339*, 135–151.

Marfin, S.S., Zvykas, A.B., Korabliova, L.A. 1988. Otchet o rezultatakh geologo-geophyzycheskikh rabot s cel'yu ocenki prognoznykh resursov severo-zapadnogo sklona Belorusko-Mazurskoy anteklizi na teritoriyi Litovskoy SSR na zheleznye rudy, provedennykh v 1982–1988 g. g (Varenskaya ploshchad'), Geolfond GGSL, Vilnius.

Marfinas, S. 1996. Report of the Varena Iron Ore deposit investigations for exploration purposes. Geology of the Varena ore-bearing area and iron ore deposit. V 2, Vilnius, Archive of the Lithuanian Geological Survey [In Lithuanian].

Marfinas, S. 1998. Report of additional investigations in south Lithuania at a scale of 1:200 000 in 1990–1992

(Dzūkija area). V 1, Vilnius, Archive of the Lithuanian Geological Survey [In Lithuanian].

Meinert, L.D. 1992. Skarns and skarn deposits. *Geoscience Canada Reprint Series 6*, 117–134.

Meinert, L.D. 1997. Application of skarn deposit zonation models to mineral exploration. *Exploration and Mining Geology 6*, 185–208.

Metz, P., Puhan, D., Winkler, H.G.F. 1968. Equilibrium reactions in the formation of talc and tremolite by metamorphism of siliceous dolomite. *Naturwissenschaften 55 (5)*, 225–226.

Montel, J., Foret, S., Veschambre, M., Nicollet, C., Provost, A. 1996. Electron microprobe dating of monazite. *Chemical Geology 131*, 37–53.

Motuza, G., Marfinas, S., Skridlaite, G., Skripkina, T. 1989. Metasomatic rocks of the Varena Iron Ore Zone in southern Lithuania. In: *Precambrian metasomatites and their mineralization*. Maskva, Nauka, 272 pp. [In Russian].

Motuza, G., Kirkliauskaitė, V. 2016. UltramaficVarėna Suite in the crystalline basement of the Southern Lithuania implications for the origin. *Baltica 29 (2),* 93–106.

Prusinskiene, S., Siliauskas, L., Skridlaite, G. 2017. Varieties and chemical composition of magnetite in the Varėna Iron Ore deposits. *Chemija 28 (1)*, 39–57.

Siliauskas, L., Skridlaite, G., Baginski, B., Whitehouse, M., Prusinskiene, S. 2018a. What the ca. 1.83 Ga gedrite-cordierite schists in the crystalline basement of Lithuania tell us about the late Palaeoproterozoic accretion of the East European Craton. *GFF 140 (4),* 332–344.

Siliauskas, L., Skridlaite, G., Whitehouse, M., Soesoo, A. 2018b. A ca. 1.89 Ga magmatic complex in eastern Lithuania: a link connecting with the domains in Estonia and Bergslagen terrane in Sweden. *Abstracts in 33rd Nordic Geological Winter Meeting*, 10th–12th January 2016, Copenhagen, Denmark, p. 59.

Skridlaite, G. 1993a. Metasomatism in the Varena Iron Ore Zone, southern Lithuania. Ph. D. Thesis, Geological Institute and University of Vilnius (1993).

Skridlaite, G. 1993b. Geochemical peculiarities of metasomatic rocks from Varensky Iron-ore zone on southern Lithuania. *Zapiski Vserossiyskogo Mineralogicheskogo Obshchestva 1*, 81–88 [In Russian].

Skridlaite, G., Motuza, G. 2001. Precambrian domains in Lithuania: evidence of the terrane tectonics, 2001. *Tectonophysics 339 (1–2),* 113–133.

Skridlaite, G., Wiszniewska, J., Duchesne, J.-C. 2003. Ferro-potassic A-type granites and related rocks in NE Poland and S Lithuania: west of the East European Craton. *Precambrian Research 124 (2–4)*, 305–326.

Skridlaite G., Bogdanova S., Page L. 2006. Mesoproterozoic events in Eastern and Central Lithuania as recorded by 40Ar/39Ar ages. *Baltica 19 (2),* 91–98.

Skridlaite, G., Bogdanova, S., Taran, L., Baginski, B. 2014. Recurrent high grade metamorphism recording a 300 Ma long Proterozoic crustal evolution in the western part of the East European Craton. *Gondwana Research 25*, 649–667.

Smith, K.L., Milnes, A.R., Eggleton, R.A. 1987. Weathering of basalt: formation of iddingsite. *Clays and Clay Minerals 35 (6),* 418–428.

Sun, M. 1957. The nature of iddingsite in some basaltic rocks of New Mexico. *American Mineralogist 42*, 525–533.

Sundblad, K., Mansfeld, J., Motuza, G., Ahl, M., Claesson, S. 1994. Geology, geochemistry and age of a Cu–Mo bearing granite at Kabeliai, Southern Lithuania. *Mineralogy and Petrology 50*, 43–57.

Vejelyte, I., Bogdanova, S., Salnikova, J., Yakovleva, S., Fedoseenko, A. 2010. Timing of ductile shearing within the Druksiai_Polotsk deformation zone, Lithuania: a TIMS U/Pb titanite age. *Estonian Journal of Earth Sciences 59*, 3–9.

Vejelyte, I., Bogdanova, S., Skridlaite, G. 2015. Early Mesoproterozoic magmatism in northwestern Lithuania: a new U-Pb zircon dating. *Estonian Journal of Earth Sciences 64 (3),* 189–198.

Widmark, E.T. 1980. The Reaction Chlorite + Dolomite = Spinel + Forsterite + Calcite + Carbon Dioxide + Water. *Contributions to Mineralogy and Petrology 72*, 175–179.

Winter, J.D. 2014. *Principles of Igneous and Metamorphic Petrology*. Pearson Education Limited, Second Edition, 738.

Zharikov, V.A., Rusinov, V.L. (eds.) 2015. *Metasomatism and metasomatic rocks*. Academy of Sciences of Russia, Institute of Geology of Ore Deposits, Petrography, Mineralogy and Geochemistry Section on Metasomatism at the Council on Mineralization and Metallogeny, 517 pp.

Supporting Online Material

http://www.gamtostyrimai.lt/uploads/documents/lediniai/Baltica/Vol-32-1-2019/09%20Baltica%202019%2032-1%20Skridlaite%20et%20al.pdf

Tables S1, S2